

Application of the Virtual Crack Closure Technique to Calculate Stress Intensity Factors for Through Cracks with an Oblique Elliptical Crack Front

September 1996

S. Fawaz

Application of the Virtual Crack Closure Technique to Calculate Stress Intensity Factors for Through Cracks with an Oblique Elliptical Crack Front

S. Fawaz

Copyright © 1996, by Delft University of Technology, Faculty of Aerospace Engineering, Delft, The Netherlands.

All rights reserved. No part of this publication may be reproduced, stored in a retrieval system or transmitted in any form or by any means, electronic, mechanical, photocopying, recording or otherwise, without the prior written permission of the Delft University of Technology, Faculty of Aerospace Engineering, Delft, The Netherlands.

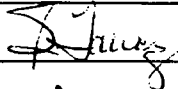
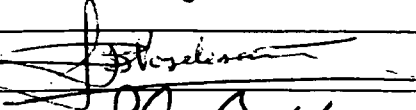
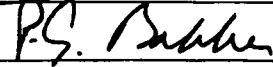
Publisher: Delft University of Technology
Faculty of Aerospace Engineering
P.O. Box 5058
2600 GB Delft
The Netherlands.
tel: (015)782058
fax: (015)781822

Date April 1996

Report LR - 805

ISBN: 90-5623-039-5

Title	:	Application of the Virtual Crack Closure Technique to Calculate Stress Intensity Factors for Through Cracks with an Oblique Elliptical Crack Front
Author(s)	:	S. Fawaz
Abstract	:	<p>Fractographic observations on fatigue tested 2024 T3 clad aluminum riveted lap-splice joints indicate oblique fronts after the initial surface or corner crack at a rivet hole has penetrated through the sheet thickness. No stress intensity factor solutions are available for this geometry subjected to remote biaxial tension, remote bending, rivet loading, and rivet interference, which are typical for a pressurized fuselage of a transport aircraft. However, comparisons are made with solutions from the literature for remote tension and bending. To reduce model generation time for each crack geometry, one finite element mesh is used to generate a model for each crack geometry for which a stress intensity factor solution is desired. In using this procedure, the original orthogonal mesh, a mesh where all of the crack plane elements are orthogonal to one another, is modified to accommodate the new crack geometries; therefore, maintaining an orthogonal crack-front mesh is not possible. The validity of the three dimensional Virtual Crack Closure Technique, 3D VCCT, with non orthogonal finite element meshes for calculating mode I stress intensity factors is assessed. Comparisons are made to existing two and three dimensional stress intensity factor solutions obtained using conformal mapping, boundary collocation, and finite element analysis. Given a sufficiently fine mesh, the 3D VCCT result is practically invariant to mesh pattern. Using the 3D VCCT with a non orthogonal mesh, a cursory sensitivity study is accomplished to assess the effect of the crack profile of a through crack on the stress intensity factor. If a through crack with an oblique elliptical shape is approximated as a straight crack, the stress intensity factors are nearly the same for remote tension but not for remote bending.</p>
Keyword(s)	:	Stress intensity factor, finite element method, finite element analysis, virtual crack closure technique, cracks, lap-splice joint, oblique, part elliptical, through, part through, three dimensional, fuselage, combined loading, tension, bending, ZIP3D, SURF3D

Date	April 1996
Prepared	S. Fawaz 
Verified	
Approved	L.B. Vogelesang 
Authorized EB	P.G. Bakker  20/09/96

Acknowledgment

I would like to thank Professor dr. ir. J. Schijve of the Faculty of Aerospace Engineering, Technical University Delft for his continued support throughout the course of this research effort in addition to his many insightful comments, notably on the more detailed aspects of this work. Additional thanks goes to Dr. James C. Newman Jr. of the NASA/Langley Research Center, Hampton, VA USA, not only for all the computer resources, both hardware and software, which made this work possible, but also for his ideas on how to approach the problem and verify the results. Finally, I am grateful to ir. A. U. de Koning of the National Aerospace Laboratory of The Netherlands for his patience in explaining the more intricate theoretical aspects of all analytical methods used in this study as well as his constructive comments given during the preparation of this report.

Table of Contents

1. Introduction.....	7
2. Background	8
2.1 Direct Methods	9
2.1.1 Crack Opening Displacement Method	9
2.1.2 Force Method	11
2.2 Indirect Methods.....	12
2.2.1 Stiffness Derivative Method	13
2.2.2 Extension of the Stiffness Derivative Method	14
2.2.3 The J-Integral.....	16
3. Methodology	18
3.1 Three Dimensional Virtual Crack Closure Technique	19
3.2 Finite Element Analysis Methodology.....	21
3.3 Finite Element Models	22
4. Validation Results.....	23
4.1 Verification of Stress State.....	24
4.2 Circular Internal Crack Embedded in an Infinite Solid Subject to Uniform Tension...	24
4.3 Cracks in Three Dimensional Finite Bodies	28
4.3.1 Center Crack Tension.....	28
4.3.2 Single Edge Crack Tension.....	28
4.3.3 Semi-Elliptical Surface Crack Subject to Tension and Bending.....	29
4.3.4 Diametrically Opposed Through Cracks at a Hole Subject to Remote Biaxial Tension, Remote Bending, and Uniform Internal Pressure	32
4.3.5 Through Cracks with an Oblique Elliptical Crack Front Subject to Remote Tension and Bending	35
4.4 Influence of a Non Orthogonal Finite Element Mesh on Stress Intensity Factors Calculated Using the 3D VCCT.....	37
4.4.1 Center Cracked Tension with Skewed Mesh at the Crack Front Subject to Remote Tension.....	39
4.4.2 Internal Elliptical Crack Embedded in an Infinite Solid Subject to Remote Tension	40
5. Application Results	43
5.1 Diametrically Opposed Through Cracks at a Hole	43
5.1.1 Biaxial Tension	43
5.1.2 Pin Loaded Hole.....	45
5.2 Effect of Oblique Crack Shape on Stress Intensity Factor.....	50
6. Conclusions.....	51
7. References	53

List of Figures

Figure 1 Diagram of an Oblique Elliptical Crack Front	8
Figure 2 Crack Opening Displacement.....	10
Figure 3 Nodal Displacements on $y = 0$ Plane at the Interface Between Layers i and $i+1$	11
Figure 4 A. Orthogonal Mesh, B. Non Orthogonal Mesh	11
Figure 5 Nodal Forces on $y = 0$ Plane at the Interface Between Layers i and $i+1$	13
Figure 6 Arbitrary Contour Around the Crack Tip Used in J-Integral	17
Figure 7 Diagram of Crack Plane Parameters Used in Calculation of the Local Strain Energy Release Rate	20
Figure 8 Baseline Finite Element Model	23
Figure 9 Comparison of Theoretical and FEA Normalized Stress in a Finite Width Plate with a Centrally Located Hole Subject to Uniform Remote Tension	24
Figure 10 Comparison of Theoretical and FEA Normalized Stress in a Finite Width Plate with a Centrally Located Hole Subject to Uniform Biaxial Tension	25
Figure 11 FE Mesh Pattern for Internal Circular Crack Embedded in an Infinite Solid	26
Figure 12 Parametric Angle Definition	26
Figure 13 Comparison of Theoretical and FEA Solutions for Circular Internal Crack Embedded in an Infinite Solid Subject to Uniform Tension.....	27
Figure 14 Comparison of CCT FEM Mode I Stress Intensity Factor Solutions	29
Figure 15 Comparison of SECT FEM Mode I Stress Intensity Factor Solutions	30
Figure 16 Comparison of Semi-Elliptical Surface Crack Subject to Tension and Bending FEM Mode I Stress Intensity Factor Solutions	31
Figure 17 Comparison of Diametrically Opposed Through Cracks at a Hole Subject to Tension	32
Figure 18 Comparison of Diametrically Opposed Through Cracks at a Hole Subject to Uniform Biaxial Tension	33
Figure 19 Comparison of Diametrically Opposed Through Cracks at a Hole Subject to Bending	34
Figure 20 Comparison of Finite Width Plate with a Centrally Located Hole Subject to Uniform Internal Pressure	34
Figure 21 Diagram of Through Crack with Oblique Elliptical Crack Front.....	35
Figure 22 Comparison of Through Cracks with Oblique Elliptical Crack Front Subject to Remote Tension.....	36
Figure 23 Comparison of Through Cracks with Oblique Elliptical Crack Front Subject to Remote Bending	36
Figure 24 Comparison of Through Cracks with Oblique Elliptical Crack Front Subject to Remote Tension and Bending	38
Figure 25 Comparison of SIF Solutions for a Semi-Elliptical Surface Crack Subject to Remote Tension and Bending	38
Figure 26 Diagram of Crack Plane of Chevron Skew Mesh with the Force and Displacement Nodes Used to Calculate K	39
Figure 27 Diagram of Crack Plane of Linear Skew Mesh with the Force and Displacement Nodes Used to Calculate K	39
Figure 28 Effect of Mesh Pattern on the Mode I Stress Intensity Factor Solution for a Straight Through Crack Subject to Remote Tension	40
Figure 29 Definition of α	41
Figure 30 Normalized Skew Ratio for Finite Element Mesh of Internal Elliptical Crack Embedded in an Infinite Body	42
Figure 31 Comparison of Elliptical Internal Crack Embedded in an Infinite Solid Subject to Uniform Tension.....	42
Figure 32 Comparison of Diametrically Opposed Straight Through Cracks from a Central Hole in a Finite Width Plate Subject to Varying Degrees of Biaxiality	44
Figure 33 Crack Opening Mode Stress Due to Biaxial Loading	44
Figure 34 Decomposition of loads in typical single shear lap-splice joint	46
Figure 35 Decomposition of Pin Loaded Hole	46
Figure 36 Effect of Rivet Load Distribution on Normalized K	49
Figure 37 Effect of Load Location on Normalized K	49
Figure 38 Sensitivity of K to Crack Shape Subject to Remote Tension	51
Figure 39 Sensitivity of K to Crack Shape Subject to Remote Tension and Bending.....	52

List of Symbols

β	Boundary correction factor
Δ	Element length normal to crack front
ν	Poisson's Ratio
π	3.14159265359
ϕ	Parametric angle of an ellipse
Φ	Complete elliptical integral of the second kind
σ_{yy}	Stress normal to crack plane
Γ	Arbitrary contour around crack tip
a	Crack depth
A_i	Constant used in COD and Force Methods
b	Finite element model half width
c	Crack length
c_1	Front surface crack length
c_2	Back surface crack length
CCT	Center Crack Tension
C_i	Constants used for partitioning nodal forces in Force Method
COD	Crack tip opening displacement
dof	Degrees of freedom
E	Modulus of elasticity
F_y	Force normal to crack plane
G_I	Mode I strain energy release rate
G_i	Local mode I strain energy release rate
h	Finite element model half height
K_I	Mode I stress intensity factor
Q	Approximation to the square of the complete elliptical integral of the second kind
r	Radial distance measured from crack front
r_D	Maximum radial distance from crack plane in COD and Force Methods
s	Crack front direction
S_{ij}	Global stiffness matrix
SECT	Single Edge Crack Tension
t	Thickness
W	Strain energy density
w_i	Element length along crack front
z_i	Coordinate direction

1. Introduction

As a result of recent catastrophic failures of transport aircraft riveted lap-splice joints due to fatigue crack growth and unstable fracture, many attempts have been made to better understand this phenomena. Toward this end, a fatigue test program of thin sheet material typically found in aircraft fuselages, 1.6 mm 2024-T3 clad aluminum alloy, with a centrally located hole subject to remote tension and bending is completed. The intent of this investigation is to gain insight on the effect of the bending stress on fatigue life and crack-front shape development. Including the bending stress is necessary in order to replicate the stress state found in lap joints. Specifically, as an aircraft is pressurized the in-plane forces resolved from the hoop stress apply an eccentric load in the lap joint. This eccentricity creates a bending moment, typically called secondary bending, and therefore normal stresses due to bending in the joint. The secondary bending has two components, a linear component due to the eccentric loading, and a non linear component due to the relatively large out of plane displacements as a result of the eccentric load application and joint geometric configuration. Müller found that the bending stresses can be as large or larger than the normal stress due to the in-plane loading.¹ For brevity, herein the normal stress due to bending and tension are referred to as bending and tensile stress respectively. The primary focus here is to calculate the influence of crack front shape on stress intensity factors for a variety of loadings, typical of those that occur in lap-splice joints.

Cracks usually nucleate as surface or corner cracks in close proximity to the rivet hole on the faying surface of the joint. As crack growth continues, the cracks penetrate the back surface, the free surface on the inside or outside of the fuselage. If the loading is pure tension, the penetrated crack length, the crack length measured from the edge of the rivet hole to the intersection of the crack front and back surface, experiences high growth rates due to the large stress gradient in the small ligament of material between the crack front and the back surface. Grandt et al. using the finite element alternating method (FEAM) verified the higher stress intensity factors, K 's, at the back surface leading to back surface crack "catch up."² The FEAM solutions agreed well with fatigue crack growth rate changes obtained during fatigue tests of polymethyl methacrylate (PMMA). In lap joints, the large secondary bending stress prohibits the back surface catch-up; therefore, a penetrated crack, as shown in Figure 1, maintains a part-elliptical, oblique, shape until rapid crack growth just prior to the onset of unstable fracture.

In service, fatigue cracks have been found which indicate a large degree of secondary bending.^{3,4} The fracture surfaces of cracks of various lengths exhibited oblique shapes indicative of penetrated surface or corner cracks subject to bending. Similar shapes are found in fatigue test specimens conducted in this study.

The three dimensional virtual crack closure technique, 3D VCCT, is used to obtain stress intensity factors, SIFs, for crack geometries and load conditions for which no published solutions are available. The structure of interest is a longitudinal riveted lap-splice joint found in the skin of a transport aircraft fuselage. This structure is

modeled by the finite element method as a finite width plate with a centrally located hole. The crack geometry of interest is a through crack which has nucleated as part through crack and grown sufficiently to penetrate the surface opposite the nucleation site. The load conditions in the structure of interest are quite complex; however, for the verification studies completed here only biaxial tension, remote bending, and rivet loading are applied.

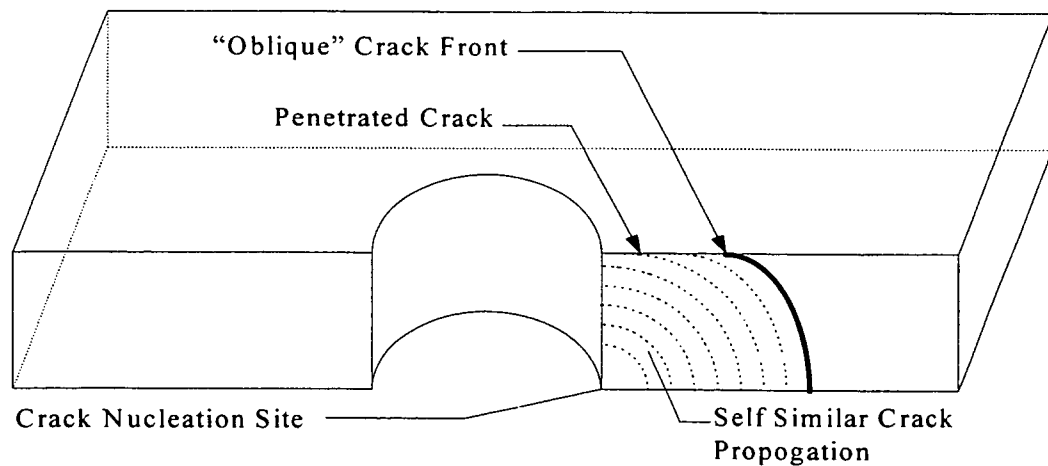


Figure 1 Diagram of an Oblique Elliptical Crack Front

The substantial emphasis is directed toward validating the 3D VCCT when used in conjunction with a finite element model that has a non orthogonal crack plane mesh. An non orthogonal mesh has elements that are not normal to adjacent elements. To appreciate the flexibility and utility of the 3D VCCT, a brief discussion of the other finite element based methods for determining K 's is found in Chapter 2. Theoretical and application considerations of the 3D VCCT are given in Chapter 1. Chapter 4 contains the results of the ten verification studies completed. Application of the 3D VCCT to obtain K 's for two new crack geometries is presented in Chapter 5, with the conclusion found in the final chapter, Chapter 6.

2. Background

To determine the closed form stress intensity factor solutions for a cracked three dimensional finite body is a difficult, and most often an intractable task; therefore alternate methods have been developed. The most prevalent for engineering applications is the finite element method (FEM). In the FEM, the K 's are determined either by direct or indirect methods. In the direct method, the stress intensity is calculated directly from the finite element solution. Three classes of elements are available in the direct approach; conventional, singularity, and hybrid. Due to the difficulties in incorporating hybrid elements in a general purpose finite element program, these elements have not been widely used; therefore, only the conventional and singularity elements are discussed here.⁵ For a thorough examination on the use of hybrid elements in obtaining fracture parameters via FEA, see reference [5]. If conventional elements are used, the stress intensity factor is estimated by evaluating

the behavior of the stresses, forces, or displacements in the vicinity of the crack tip, which are known from the finite element solution, and then extrapolating back to the crack tip. The force and crack opening displacement methods are the most prevalent implementations of this extrapolation technique. When singularity elements are used, the stress intensity factor is calculated directly. The indirect methods use nodal information, displacements and forces, to obtain the energy release rate which is then used to calculate K. Examples of indirect methods are the virtual crack closure technique, equivalent domain integral (three dimensional extension of the J-integral), and the stiffness derivative method. In addition, de Koning and Lof extended the stiffness derivative approach by making use of the stress intensity rates for a given crack extension.

Note, in a finite element model the non-singular strain terms can only approximately describe the singularity at the crack tip resulting in an underestimation of the stress intensity factor. Further, it should be noted that K values calculated from the singular part of the interpolation functions of such elements are also inaccurate because of the presence of non zero nonsingular terms in their interpolation functions.⁶ Therefore, the use of singularity elements in the direct or indirect methods is beneficial.⁷ The method used in this investigation is the three dimensional virtual crack closure technique which is discussed in detail in Chapter 3, however, the various other methods mentioned above are briefly discussed in the following sections.

2.1 Direct Methods

In a displacement finite element formulation, the fundamental result of solving the system of equations are the nodal displacements from which the nodal forces, stresses, and strains are calculated. The direct method of obtaining the stress intensity factor via FEA is attractive by making use of the standard output from a general purpose finite element program. However, in commercial finite element packages, evaluation of fracture parameters, K, may not be implemented; therefore, significant post processing of the standard output must be completed in order to extract K. The two direct methods reviewed in the proceeding sections are the crack opening displacement and force methods with a more comprehensive discussion of direct methods available in reference [5].

2.1.1 Crack Opening Displacement Method

Using the crack opening displacements (COD), as seen in Figure 2, from finite element analyses (FEA), the stress intensity factor is derived from the following plane strain relation.⁸

$$COD = 2v = \frac{8K_I}{E} \sqrt{\frac{r}{2\pi}} (1 - \nu^2) + O\left(r^{\frac{3}{2}}\right) + \dots \quad (1)$$

where

$K_I \equiv$ Mode I Stress Intensity Factor

$E \equiv$ Modulus of Elasticity

$r \equiv$ Normal distance from crack front to displacement node

$\nu \equiv$ Poisson's ratio

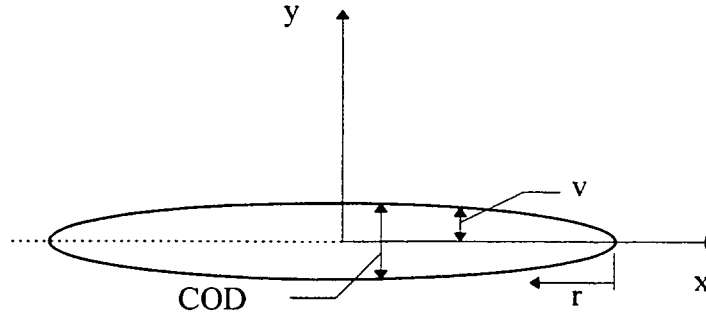


Figure 2 Crack Opening Displacement

Upon solution of the finite element model (FEM), all integration point values are known, e.g.; displacements, forces, strains, and stresses. Then Eqn. (1) is rearranged in the form,

$$\frac{Ev}{\sqrt{\frac{r}{2\pi}} 4(1-\nu^2)} = K_I + A_1 r + \dots \cong K_I + A_1 r \quad (2)$$

where K_I is as defined previously and A_1 is an unknown constant. By substituting the COD at a given r location for several locations in the crack wake normal to the crack front as shown in Figure 3, K_I and A_1 can be determined by a least squares linear regression.⁸ The singular portion of the crack opening stresses, σ_{yy} , in the crack plane vary with $1/\sqrt{r}$ for small values of r ; therefore, care must be taken in choosing the maximum r . To better represent this variation, quadratic not linear elements should be used near the crack tip. In addition, since the constants are evaluated at nodes j , K_I is not explicitly calculated, but must be extrapolated back to the crack tip from the values at nodes j . By definition of distance from the crack front, r , the COD method is not easily implemented with non orthogonal meshes. Classification of a mesh as being orthogonal or non orthogonal depends on the orientation of the elements adjacent to the crack front on the crack plane. The difference between the two mesh types is quite evident as seen in Figure 4 where the elements surrounding the crack front in Figure 4A have sides normal and parallel to the crack front; conversely, in Figure 4B, orientation of the element sides is arbitrary. At a given location along the crack front for which K is desired, the displacements at several distances, r , normal to the crack front on the crack surface are needed; therefore, if no nodes are located at r locations, the displacements must be interpolated from those displacements at neighboring nodes.

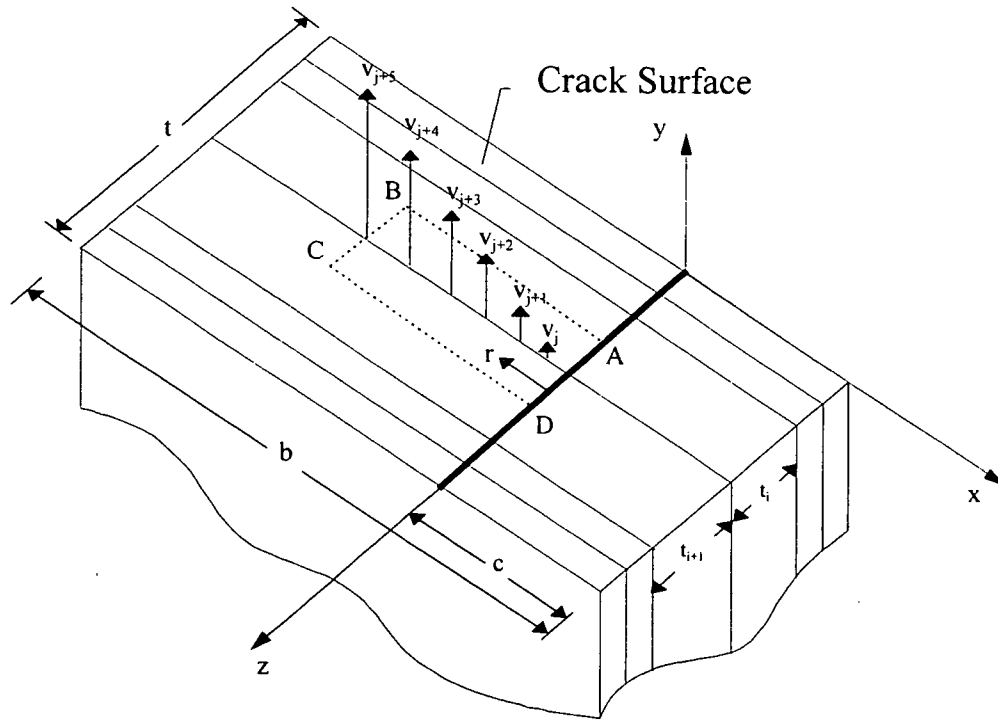


Figure 3 Nodal Displacements on $y = 0$ Plane at the Interface Between Layers i and $i+1$

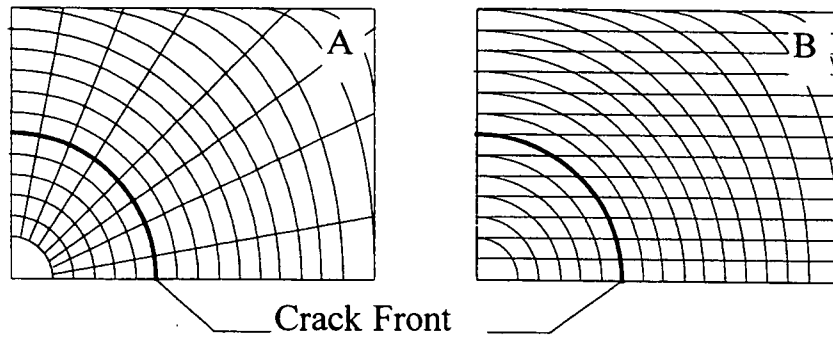


Figure 4 A. Orthogonal Mesh, B. Non Orthogonal Mesh

2.1.2 Force Method

The force method offers more generality in that unlike the COD method does not require an a priori assumption of plane stress or plane strain.⁹ Similar to the COD method, if singularity elements are used the $1/\sqrt{r}$ stress singularity is obtained by placing the singularity elements on the crack front and K is then calculated directly. Even though K can be calculated directly from the singularity elements not all singularity elements are formulated with this capability, the following outlines an extrapolation procedure to evaluate K when using singular or non singular elements.

Assuming a two dimensional stress state is valid along every infinitesimal portion of the crack front, the normal stress perpendicular to the crack front is written as

$$\sigma_y = \frac{K_I}{\sqrt{2\pi r}} + A_1 r^{\frac{1}{2}} + A_2 r^{\frac{3}{2}} + \dots \quad (3)$$

where K_I and A_1 are as defined in the COD method.⁹ The total force normal to the crack plane, over an area bounded by $z_1 \leq z \leq z_2$ and $0 \leq r \leq r_D$ can be represented as

$$F_y = \int_{z_1}^{z_2} \int_0^{r_D} \sigma_y dr dz \quad (4)$$

By substitution of Eqn. (3) in Eqn. (4), the total force is approximated as,

$$F_y = \frac{K_I}{\sqrt{2\pi}} 2\sqrt{r_D} (z_2 - z_1) + A_1 (z_2 - z_1) + \dots \quad (5)$$

$$F_y \cong \frac{K_I}{\sqrt{2\pi}} 2\sqrt{r_D} (z_2 - z_1) + A_1 (z_2 - z_1)$$

The nodal forces in the region enclosed by ABCD, shown in Figure 5, are known from the FEA and are used with Eqn. (5) to solve for K_I and A_1 using a least squares linear regression. In other words, a node in the region ABCD is located a distance r from the crack front with a force normal to the crack plane, F_j , which are substituted into Eqn. (5) resulting in an equation in terms of K_I and A_1 . Just as in the COD method, K is not explicitly calculated, but extrapolated from the values calculated at nodes j ; therefore, Eqn. (5) is applied at several nodes in close proximity to the crack front to increase the accuracy of the linear regression and extrapolation.

Through numerical experimentation, Raju and Newman have found consistent K values when Eqn. (5) is used for five forces and the maximum value of r_D is less than $a/10$ where a is the crack depth of a semi-elliptical crack or crack length for a straight crack.⁹ Similar to the displacements used in the COD method, the nodal forces used in calculating K must come from nodes normal to the crack front. This condition restricts use of non orthogonal meshes for K calculations with this method.

2.2 Indirect Methods

In general, the indirect methods determine the stress intensity factor from the elastic energy release rate. The elastic energy release rate can be obtained by determining the changes in compliance, stiffness, or energy available for crack growth during a given crack extension; in addition, the J-integral can also be used since J is equal to the

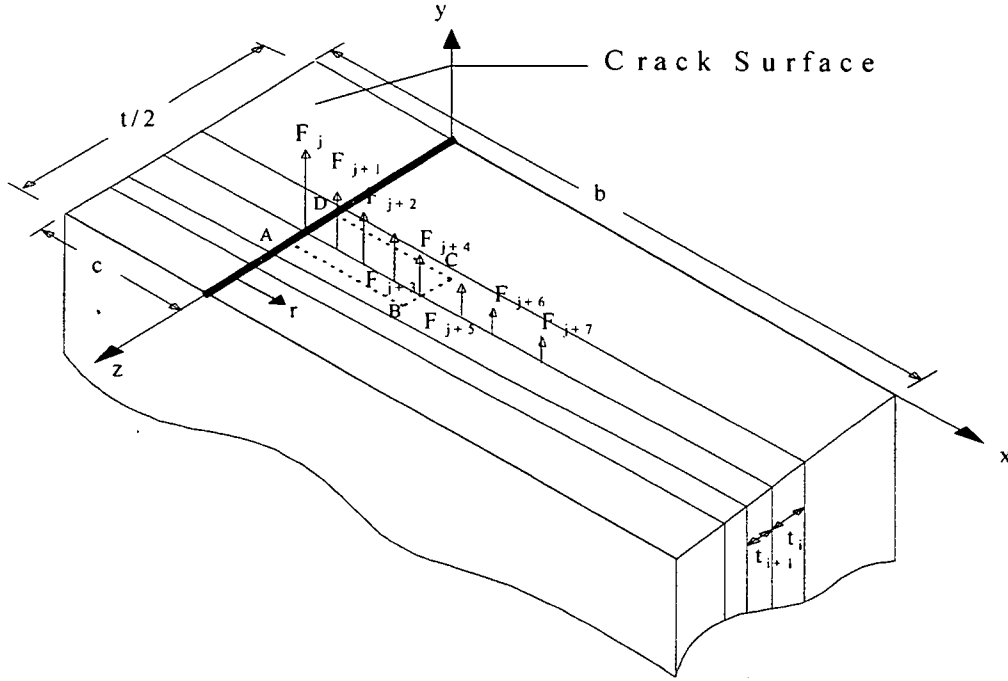


Figure 5 Nodal Forces on $y = 0$ Plane at the Interface Between Layers i and $i+1$

elastic energy release rate for linear elastic behavior. Due to additional post processing of displacement data required by the compliance method, it has not received wide spread use and is not discussed here.^{5,10,11} The stiffness derivative method, a variation of the stiffness derivative method developed by de Koning and Lof, and the J-integral are briefly discussed.

2.2.1 Stiffness Derivative Method

The stiffness derivative method independently developed by Parks and Hellen obtains K by calculating the change in the element stiffness matrices at the crack tip.^{12,13} In a finite element solution, the potential energy is expressed as

$$P = \frac{1}{2} \{u\}^T [K] \{u\} - \{u\}^T \{f\} \quad (6)$$

where

- $\{u\} \equiv$ Nodal displacement vector
- $[K] \equiv$ Global stiffness matrix
- $\{f\} \equiv$ Prescribed nodal forces

The strain energy release rate is obtained by differentiating the potential energy with respect to the crack length which yields

$$\frac{\partial P}{\partial c} = \frac{\partial \{u\}^T}{\partial c} [[K]\{u\} - \{f\}] + \frac{1}{2} \{u\}^T \frac{\partial [K]}{\partial c} \{u\} - \{u\}^T \frac{\partial \{f\}}{\partial c} \quad (7)$$

where the first term on the right hand side of Eqn. (7) is exactly zero by the finite element solution.¹² The strain energy release rate is now represented by

$$\frac{\partial P}{\partial c} = \frac{1}{2} \{u\}^T \frac{\partial [K]}{\partial c} \{u\} - \{u\}^T \frac{\partial \{f\}}{\partial c} \quad (8)$$

The partial derivative of the global stiffness matrix with respect to the crack length represents the change in the former per unit crack advance. In application, the crack advance is provided by moving the crack tip nodes an amount specified by the analyst. By further ignoring body forces and crack face loadings resulting in loading only by remote surface tractions, Eqn. (8) reduces to

$$\frac{\partial P}{\partial c} = \frac{1}{2} \{u\}^T \frac{\partial [K]}{\partial c} \{u\} \quad (9)$$

Eqn. (9) is the fundamental relation used by Parks and Hellen to introduce their technique. To implement the differential stiffness method, the global stiffness matrix is written in terms of the element stiffness matrices. In their development, Parks and Hellen prove only the elements on the crack front contribute to the change in the global stiffness matrix thereby greatly simplifying evaluation of Eqn. (9). Unfortunately, wide spread use of this technique remains limited due to the complexity of implementation into a general purpose finite element code. For further information on the development, application, and accuracy of the derivative stiffness method, see references [12] - [14].

2.2.2 Extension of the Stiffness Derivative Method

Stress intensity variations along three dimensional crack fronts have been calculated by de Koning and Lof using the stiffness derivative method to obtain stress intensity rates along the crack front.¹⁵ Their formulation is driven by the desire to obtain stress intensity factors for numerous crack lengths from one finite element analysis. From known analytical solutions, the dependency of the stress intensity distribution on the crack size and shape parameters for a wide range of crack sizes can be approximated by the following linear relation.¹⁵

$$K_i = K_i^o + \frac{\partial K_i^o}{\partial a_j} \Delta a_j \quad (10)$$

where

K_i^o \equiv Stress intensity factor at a given position along the reference crack front

$\frac{\partial K_i^o}{\partial a_j}$ \equiv Stress intensity rates

Δa_j \equiv Crack size increment

The variation of the crack front in the finite element model is done by shifting the corner nodes of the crack front elements to obtain the new crack front shape and size. The direction of the shift is normal to the reference crack front.¹⁵ The key to using this method is accurately calculating the stress intensity rates which can be derived from the displacement field in the vicinity of the crack front given by the following plane strain relation.

$$K_i = \frac{v_i E}{2(1-\nu^2)} \sqrt{\frac{2\pi}{r_i}} \quad (11)$$

where

v_i \equiv One half the crack opening displacement

r_i \equiv Distance to the crack front

Both v_i and r_i are measured in an intersection perpendicular to the crack front at the corner node location, i . Then the stress intensity rate is obtained from Eqn. (11) by

$$\frac{\partial K_i}{\partial a_j} = \frac{E}{4(1-\nu^2)} \sqrt{\frac{2\pi}{r_i}} \frac{\partial v_i}{\partial a_j} \quad (12)$$

$$\frac{\partial K_i}{\partial a_j} = \frac{K_i}{v_i} \frac{\partial v_i}{\partial a_j} \quad (13)$$

As the crack front nodes shift, the distance r_i is not affected since all the nodes in an intersection normal to the crack front are assumed to shift the same amount. In Eqn. (13) at node i , the crack opening displacements, v_i , are known from the finite element solution and the stress intensity factor, K_i , can be obtained using standard procedures like those mentioned previously. The second term in Eqn. (13) is

generated using a stiffness derivative method similar to the one described previously. From the displacement equilibrium equation,

$$\frac{\partial v_i}{\partial a_j} = S_{ki}^{-1} \left[\frac{\partial S_{kl}}{\partial a_j} v_l \right] \quad (14)$$

where

$S_{ki}^{-1} \equiv$ Inverse of the stiffness matrix

The first term inside the brackets is available from the Choleski decomposition of the system matrix which is calculated during the normal finite element solution procedure.¹⁵ From this straight forward procedure, the stress intensity rates can then be calculated without a considerable increase in computational effort.

The main benefit of this method is the ability to accurately extrapolate numerous stress intensity factors from one finite element analysis. The procedure outlined above is readily applicable to three dimensional cracks, for a detailed description see reference [15]. De Koning and Lof showed that with a relatively coarse mesh extrapolated K's were within 2% of the closed form solution for a through crack in an infinite plate with 31% crack growth with respect to the reference crack length. In a three dimensional analysis a penny shaped central crack in a prismatic rectangular bar subject to remote tension was extended to an ellipse with the K's extrapolated using Eqn. (10). The accuracy was within 2% of a new three dimensional FEA for the exact elliptical crack front. The extension of the penny crack to the ellipse represents 17% crack growth with respect to the reference crack length.

2.2.3 The J-Integral

Traditionally, the J-integral is of interest for those crack configurations where the plasticity effects are not negligible. In this case, the elastic strain energy release rate, G, being based on the elastic stress field is inadequate in describing the energy release rate. The J-integral can then be used to determine the energy release rate. In trying to avoid solution of the complex, detailed boundary value problem associated with strain concentration fields near cracks, Rice identified the J-integral (a line integral) which has the same value for all paths surrounding the tip of a notch in a two dimensional strain field.^{16,17} As defined along an arbitrary contour, Γ , around the crack tip, see Figure 6, the J-integral is represented by,^{17,18}

$$J = \int_{\Gamma} \left[W dy - \mathbf{T} \frac{\partial \mathbf{u}}{\partial x} \right] ds \quad (15)$$

where

$W \equiv$ Strain energy density per unit volume

$\mathbf{T} \equiv$ Traction vector acting along outward normal to Γ

$\mathbf{u} \equiv$ Displacement vector in the x-direction

$ds \equiv$ Arc length on Γ

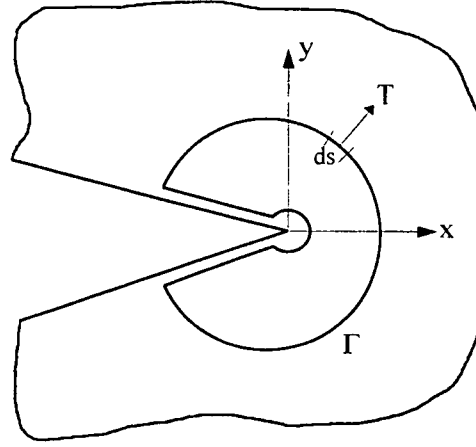


Figure 6 Arbitrary Contour Around the Crack Tip Used in J-Integral

For a linear elastic material, the J-integral is equal to the elastic energy release rate,

$$J = G \quad (16)$$

Now the J-integral can be related to the stress intensity factor in view of Irwin's assertion that the energy lost in extending the crack some distance, Δc , is equal to the work required to close the crack to its original length. This relation in polar coordinates with the origin at the crack tip takes the following form.²³

$$G_I = \lim_{\Delta c \rightarrow 0} \frac{1}{2\Delta c} \int_0^{\Delta c} \sigma_y(r, 0) \bar{v}(\Delta c - r, \pi) dr \quad (17)$$

where

$\sigma_y \equiv$ stress distribution ahead of crack front

$\bar{v} \equiv$ displacement distribution behind crack front

$r \equiv$ distance normal to crack front

For opening mode, mode I, substitution of Westergaard's solution for the stress and displacements in the vicinity of a crack into Eqn. (17), where E is the modulus of elasticity, yields

$$G_I = \frac{K_I^2}{E}(1-\nu^2) \Rightarrow K_I = \sqrt{\frac{G_I E}{1-\nu^2}} \quad \text{plane strain} \quad (18)$$

$$G_I = \frac{K_I^2}{E} \Rightarrow K_I = \sqrt{G_I E} \quad \text{plane stress}$$

The key to using the J-integral with the finite element method to obtain stress intensity factors is choosing a contour such that Eqn. (15) can be evaluated using the element stresses and displacements readily available from a standard finite element solution. As one might expect, choosing an appropriate contour, surface for three dimensional analyses, is paramount. Since the J-integral is based on the conservation of energy, the material volume enclosed by the integration surface must be in equilibrium, thus maintaining the energy balance. If the surface intersects an element, equilibrium is not guaranteed; therefore, choosing a path along the element boundaries is recommended.¹⁹ Furthermore, extrapolation errors are avoided if the integration surface is defined by the integration points of the elements and not the nodes.

By substituting $\mathbf{T} = \sigma \mathbf{n}$ in Eqn. (15), the J-integral is now in terms of the element stresses and displacements.

$$J = \int_{\Gamma} \left(W \mathbf{n} - \sigma \frac{\partial \mathbf{u}}{\partial \mathbf{x}} \mathbf{n} \right) ds \quad (19)$$

where σ is the element stress tensor with all other quantities as defined in Eqn. (15).

Using the stress and displacements at the integration points for a given element on the integration surface, the local J-integral is calculated using Eqn. (19). The strain energy, W , and displacement derivatives, $\partial \mathbf{u} / \partial \mathbf{x}$, use the FEA output; whereas, the normal vector, \mathbf{n} , uses the nodal point coordinates. For a numerical procedure to determine these three quantities see reference [19]. The local J-integral must now be calculated for those elements which are inside and adjacent to the integration surface. The final step is to define how the J-integral varies along the integration surface. Bakker found that a simple average of the J-integral values between adjacent elements is adequate and that when using quadratic elements with third order gaussian integration little improvement is seen when using a more elaborate interpolation method.¹⁹ For further discussion on evaluating the J-integral in a finite element model see references [8], [20], [21].

3. Methodology

The principal obstacle inhibiting use of the COD, force, and derivative stiffness methods is not related to accuracy but application. The COD and force methods require the elements to be normal to the crack front which restricts the types of crack geometries that can be solved. For example, creating elements normal to a curved crack front is time consuming and may not be possible at locations where the crack

intersects a free surface. Although the derivative stiffness method does not require a specific element orientation with respect to the crack front, the solution algorithm to calculate the stress intensity factors is not easily incorporated into a general purpose finite element code. Therefore, the desire to have a general purpose finite element code that can also calculate stress intensity factors for complex crack shapes served as the impetus for the development of the three dimensional Virtual Crack Closure Technique (3D VCCT). Furthermore, the 3D VCCT can be easily used with any commercially available finite element analysis software.

3.1 Three Dimensional Virtual Crack Closure Technique

The 3D VCCT used for calculation of stress intensity factors is based on Irwin's crack closure integral.²² The formulation for use with FEA is originally addressed by Rybicki and Kanninen for two dimensions and extended to three dimensions by Shivakumar, Tan and Newman.^{23,24} Extending Irwin's relation, Eqn. (17), to three dimensional bodies with the intent of application to the finite element method, Shivakumar et al. proposed²⁴

$$G_i = \frac{1}{2w_i\Delta} \int_{s_{i-1}}^{s_{i+1}} \int_0^\Delta \sigma_y(r,s) \bar{v}(\Delta - r,s) dr ds \quad (20)$$

where

- w_i \equiv Element length along crack front
- Δ \equiv Element length on each side and normal to crack front
- σ_{yy} \equiv Stress distribution ahead of crack front
- \bar{v} \equiv Displacement distribution behind crack front
- r \equiv Distance normal to crack front
- s \equiv Distance along crack front

The limits of integration for s in Eqn. (20) are such that the force contributions of the elements adjacent to element i are included. Figure 7 illustrates those parameters used in the calculation of G_i . Application of Eqn. (20) presumes a continuous crack front can be approximated by discrete segments as typically found in FEMs. The right hand side of Eqn. (20) is equivalent to the product of the nodal forces ahead of the crack front and the nodal displacements behind the crack front for the i^{th} segment with contributions from elements on each side of the crack front.²⁴ Eqn. (20) is in terms of the i^{th} segment alone and a typical FEA solution gives nodal quantities, force and displacement contributions from all elements connected to a given node. As a consequence, a method of partitioning the nodal forces must be devised. Assuming the nodal forces are proportional to the element length normal to the crack front, the strain energy release rate for an eight node element is written as

$$G_i = \frac{1}{2w_i\Delta} \sum_{j=1}^2 C_j F_j \bar{v}_j \quad (21)$$

where

$$C_1 = \frac{w_i}{w_{i-1} + w_i}$$

$$C_2 = \frac{w_i}{w_i + w_{i+1}}$$

Note, the forces come from nodes on the crack front, and the displacements from nodes behind the crack front.

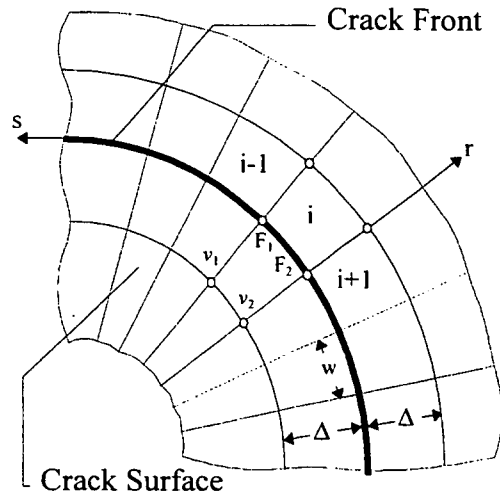


Figure 7 Diagram of Crack Plane Parameters Used in Calculation of the Local Strain Energy Release Rate

For a more complete discussion and use of this method with higher order elements see reference [24]. Eqn. (21) is exact for a uniform stress field and approximate for a non uniform stress field.²⁴ As described above, the 3D VCCT appears to require an orthogonal mesh neighboring the crack front; however, looking more closely at Eqn. (20) orthogonality is not essential. The local strain energy release rate is the virtual work required to close the crack over a surface area, $w_i\Delta$, and for application to FEA is the element area in the crack plane. The normality requirements in Eqn. (20) is only assumed to simplify the original derivation. The only information related to element shape is used to correctly partition the nodal forces, which again, have no normality requirement. Eqns. (17), (21), (22) are used for the full field strain energy release rate which translates to one FEA to obtain G_I , G_{II} , and G_{III}

3.2 Finite Element Analysis Methodology

The finite element analysis codes used, ZIP3D and SURF3D, were developed by the NASA Langley Research Center specifically for obtaining fracture parameters, strain energy release rate, stress intensity factor, and J-integral, in three dimensional elastic and elastic-plastic bodies.^{8,25} In addition, uncracked bodies may also be analyzed to obtain stress, strain, and displacement fields. Although incorporation of linear elastic fracture mechanics analysis capability in commercially available finite element packages is increasing, they are usually restricted to analysis of two dimensional bodies or for evaluating only the total strain energy release rates of a three dimensional body.²⁵ The code has only one element type, eight noded isoparametric solid, and is capable of using a special reduced shear integration scheme for bending dominant problems. The isoparametric element formulation is used to define the shape functions which are then used to create the stiffness matrix.^{26,27,28,29} Linear finite elements are arbitrarily stiff in the transverse direction if all stresses are included in the integration, full integration, therefore, by reducing the number points for shear integration the flexibility of the model is increased. Several researchers have given more detailed explanations of the applicability and benefits of reduced integration.^{26,27,28,29,30,31}

The models can be loaded at the nodes by applying displacements, concentrated loads, or surface tractions which offers great flexibility in combined loading analyses. By superposition, the contribution of each load case to the three fracture modes, modes I, II, and III, is determined. The total mode I stress intensity factor is simply the addition of the individual stress intensity factors which can be expressed in equation form as

$$K_{TOTAL} = \sum_{i=1}^n K_i \quad (22)$$

For example, the stress intensity for a plate subject to remote tension and bending is obtained by loading the model in tension then bending and extracting the K's for each analysis individually. Expanding to the basic definition of stress intensity yields

$$K_{TOTAL} = \left(\sum_i^n \beta_i \sigma_i \right) \sqrt{\pi a} \quad (23)$$

where $\beta_i \equiv$ Boundary correction factor for each load condition
 $\sigma_i \equiv$ Remote stress for each load condition
 $a \equiv$ Crack length

Although not employed here, crack extension analyses are also possible for cracks with straight profiles. For additional discussion of the solution methods used in each code, see references [8] and [25].

3.3 Finite Element Models

Many commercially available finite element preprocessors have the capability to write node and element information to simple text files which is the format requirement for both ZIP3D and SURF3D. All models in this study were generated using McNeal-Schwendler Corporation MSC/PATRAN version 1.4.2. As can be expected, much care must be exercised in generating the mesh pattern on and near the crack plane. As mentioned previously, the COD and force methods require orthogonal meshes around the crack front to obtain accurate K solutions. No such stipulation is known for the 3D VCCT; therefore both orthogonal and non orthogonal meshes are generated. If a particular K solution is desired for one geometry, then maintaining an orthogonal mesh is quite simple. However, if multiple solutions are obtained from modifying one mesh, especially in the case of oblique crack fronts, orthogonality cannot be sustained due to the changing geometric requirements. The orthogonality requirement is discussed in further detail in the proceeding sections.

Finite element models were generated to develop K solutions for a circular internal crack embedded in an infinite solid subject to uniform tension, center crack tension (CCT), single edge crack tension (SECT), semi-elliptical surface crack subject to tension and bending, diametrically opposed through cracks at a hole subject to tension and bending, and semi-elliptical crack in post penetration subject to tension and bending. All models are constructed employing symmetry arguments where available. Except for the circular internal crack embedded in an infinite solid which is modeled with one eighth of the plate; in general, only one quarter of a plate, shown in Figure 8, is required to model the entire plate. Symmetry planes are located at $x = 0$ and $y = 0$; in addition, for plane strain analyses, $z = 0$ and $z = t$ are also fully constrained. Furthermore, sufficient global dimensions are used to avoid perturbations of the stress field due to mesh transitions, load application, and boundary conditions. Therefore, the following ratios are maintained for all models.

$$\frac{h}{b} \geq 1.5 \quad \frac{t}{b} \leq 0.2 \quad \frac{c}{b} \leq 0.5 \quad (24)$$

The computer requirements for generating the models and K solutions are quite modest. All preprocessing and model generation/manipulation is done on Sun Microsystems SPARC 5 and SPARC 20. The finite element solutions are completed on both a Digital Equipment Corporation DEC 3000/900 single processor workstation and Cray Research Corporation CRAY YMP eight processor super computer. All of the software and computers, except the SPARC 5, were provided by Dr. James C. Newman, Jr. of the NASA Langley Research Center. To give an idea of the time for an elastic solution of a representative 55,000 degrees of freedom model, the DEC 3000/900 requires approximately 1900 CPU seconds; whereas the CRAY YMP only 300. This is simply a qualitative measure since CPU time is heavily dependent on system configuration, hardware resources, and assigned processing priorities. With respect to the precision of each machine, both use 64 bit double precision resulting in 15 significant digits.

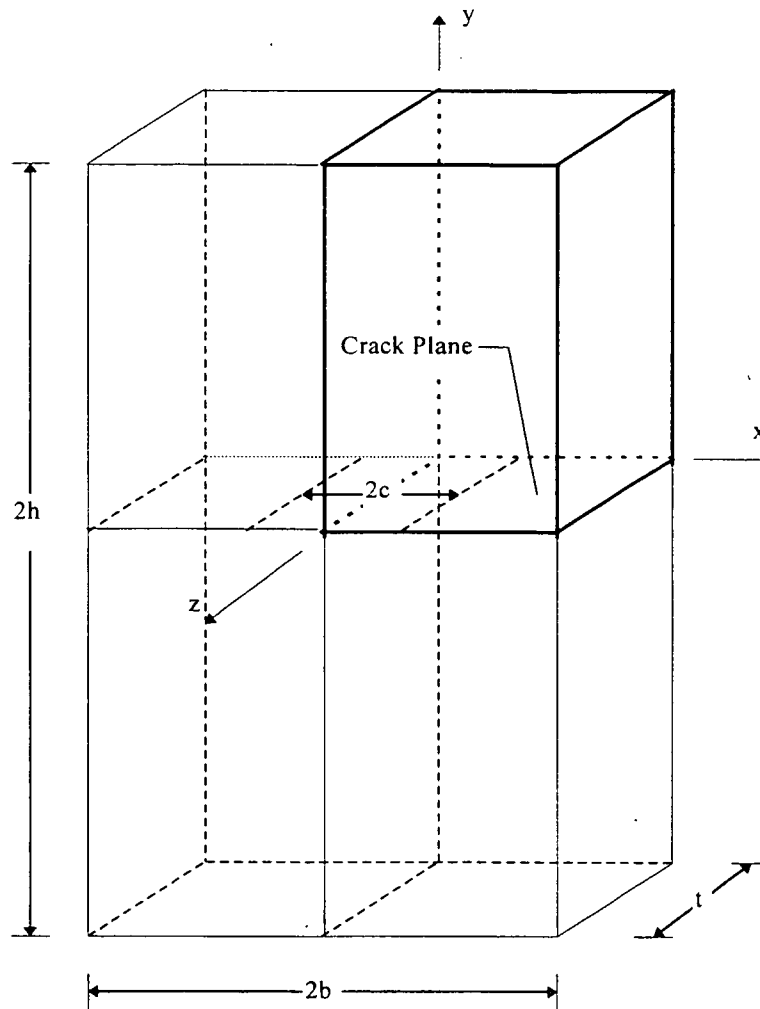


Figure 8 Baseline Finite Element Model

4. Validation Results

In order to evaluate the accuracy of a finite element model with regard to the degree of discretization error, convergence studies are usually employed. In view of the various crack geometries of interest, the preprocessing requirements for a convergence study are prohibitive; therefore, the model results are compared to known stress and stress intensity solutions. Since mode I stress intensity solutions are of prime interest, the normal stress in the y-direction, σ_{yy} , are examined thoroughly. For example, for a model to be used to generate K_I solutions for a CCT specimen, a stress analysis without a crack is performed. By constraining all of the nodes on the crack plane, $y = 0$, no perturbations of the stress field in the y-direction are acceptable when away from the point of load application. For models with a centrally located hole in a plate, the stress concentration factor at the edge of the hole is an additional parameter used for model verification. Furthermore, closed form stress intensity solutions when available are also used for confirmation of model adequacy.

4.1 Verification of Stress State

For all of the models used to generate K_I solutions for through the thickness cracks whether straight or oblique, the stress analysis with no crack present yielded no deviation in the stress field from the theoretical solution within the limits of computer precision.³² For the models with centrally located holes, the stress distribution in the net section was also used. Figure 9 and Figure 10 illustrate the accuracy of the present solution. In a displacement formulation finite element analysis, solution of the system of equations yields the displacements of the unconstrained degrees of freedom from which the stresses are calculated. Integration of the stiffness matrix occurs by numerical integration at the Gauss points of the elements. By using the interpolation (shape) functions, the nodal quantities are then extrapolated. The small deviation from the theoretical value at the root of the notch, $x/r = 1$, plotted in Figure 9 and Figure 10 is due to the extrapolation of the stress from the Gauss points to the nodes. Recall, the 8 noded isoparametric brick elements being used here are linear elements; thus extrapolation is also linear.

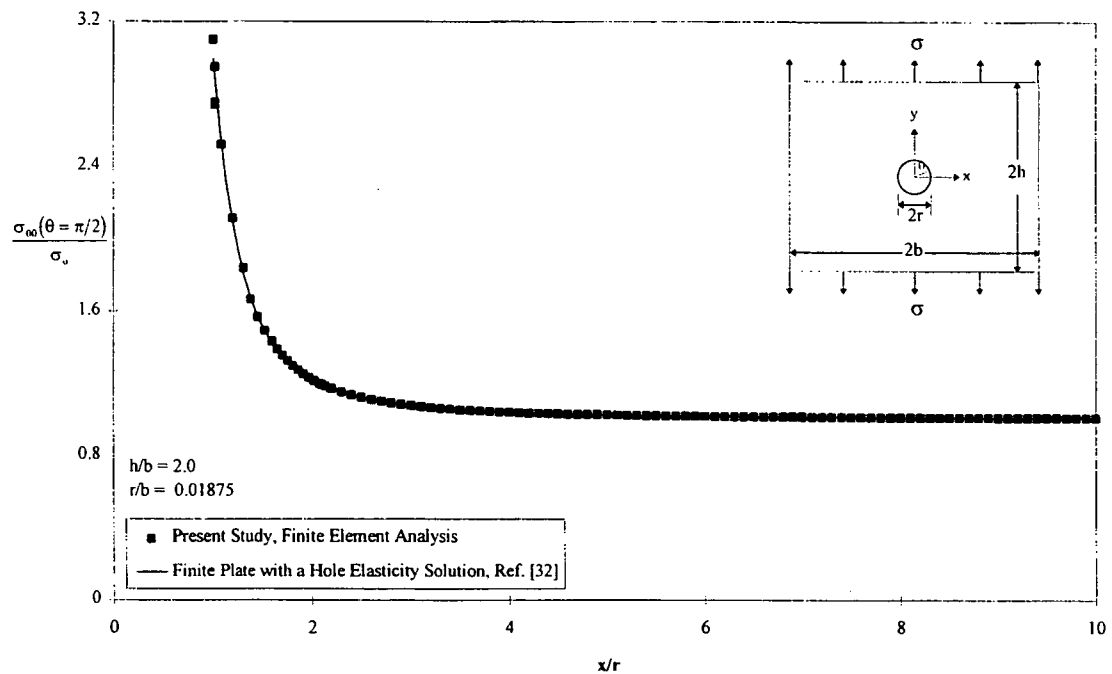


Figure 9 Comparison of Theoretical and FEA Normalized Stress in a Finite Width Plate with a Centrally Located Hole Subject to Uniform Remote Tension

4.2 Circular Internal Crack Embedded in an Infinite Solid Subject to Uniform Tension

This crack configuration was analyzed first since there is a closed form solution available for comparison. In addition, the crack does not intersect a free surface

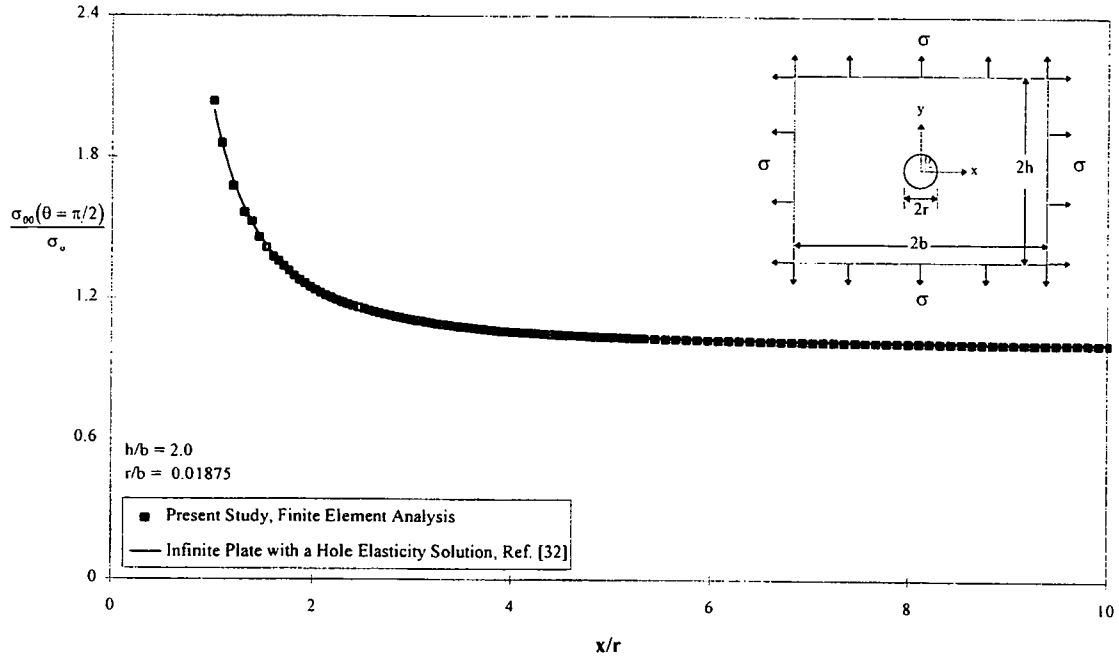


Figure 10 Comparison of Theoretical and FEA Normalized Stress in a Finite Width Plate with a Centrally Located Hole Subject to Uniform Biaxial Tension

where the calculation of the strain energy release rate is questionable. The finite element model created to generate K solutions for this crack geometry has 6032 elements, 7182 nodes and 21,546 degrees of freedom. The crack plane mesh, $y = 0$, is circular at the crack location to better represent the circular front as shown in Figure 11. Due to the symmetry of the problem only one eighth of the plate is modeled and a unit stress is applied at the top of the plate. The mode I stress intensity factors have been normalized using the following relation.

$$\beta = \frac{K}{\sigma \sqrt{\pi a}} \quad (25)$$

Herein, all stress intensity solutions obtained are assumed to be mode I and plane strain is assumed when converting strain energy release rates to stress intensity factors. In addition, for all models having a crack intersect a free surface, plane stress is assumed at the free surface to accommodate for the changes in constraint and crack closure at the free surface. Obviously, a circular internal crack embedded in an infinite body doesn't intersect a free surface; therefore, plane strain K 's are calculated along the entire crack front. Note, commonly K 's for semi-elliptical cracks are depicted as a function of the parametric angle, ϕ , of an ellipse as defined in Figure 12. Since a circle has the same functional form as an ellipse, the same convention is used.

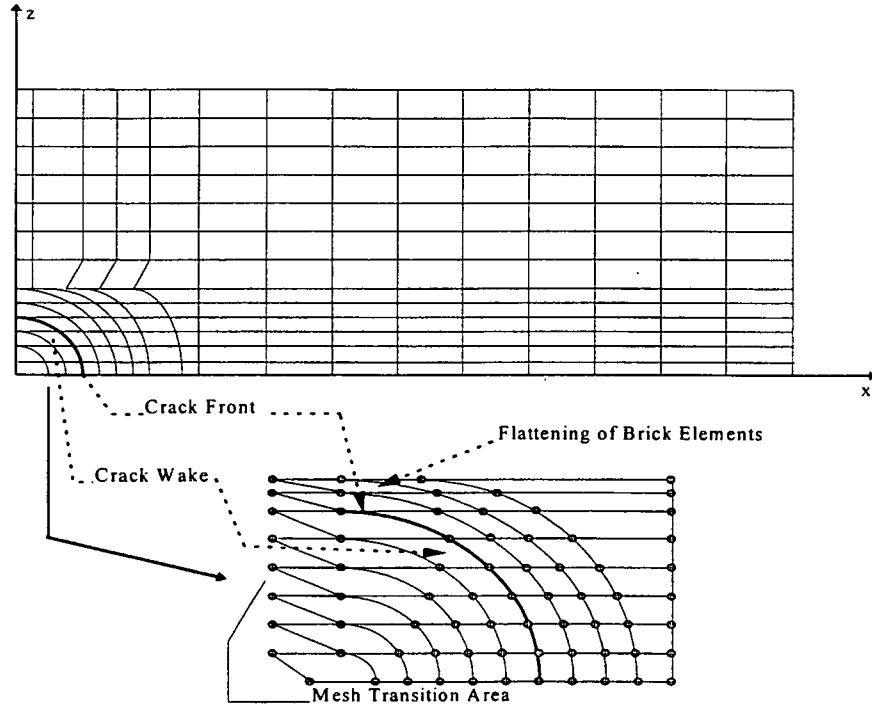


Figure 11 FE Mesh Pattern for Internal Circular Crack Embedded in an Infinite Solid

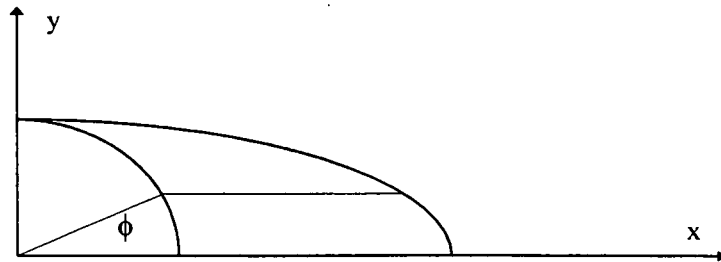


Figure 12 Parametric Angle Definition

Sneddon derived the solution of a circular crack in an infinite solid.³³

$$K = \frac{2}{\pi} \sigma \sqrt{\pi a} \quad (26)$$

A comparison of the FEA results and theoretical solution is made in Figure 13. At first glance, the variation between the FEA results and theoretical solution in the range $0 \leq 2\phi/\pi \leq 0.7$ appears extreme. However, the crack plane finite element mesh explains much of the variation seen in this range of ϕ . The somewhat regular variation indicates large mesh transitions where elements on one side of the crack front are of different size relative to the adjacent element. Recall, G is calculated from

nodal forces on the crack front and displacements one element behind the crack front. At the mesh transitions, the assumption is made that the nodal quantities are proportional to the element size; therefore in calculating G an average area is used in addition to scaling the forces as a function of the element size. As will be seen in results presented later, this variation disappears with a more uniform mesh where the element size transitions at the crack front are minimized.

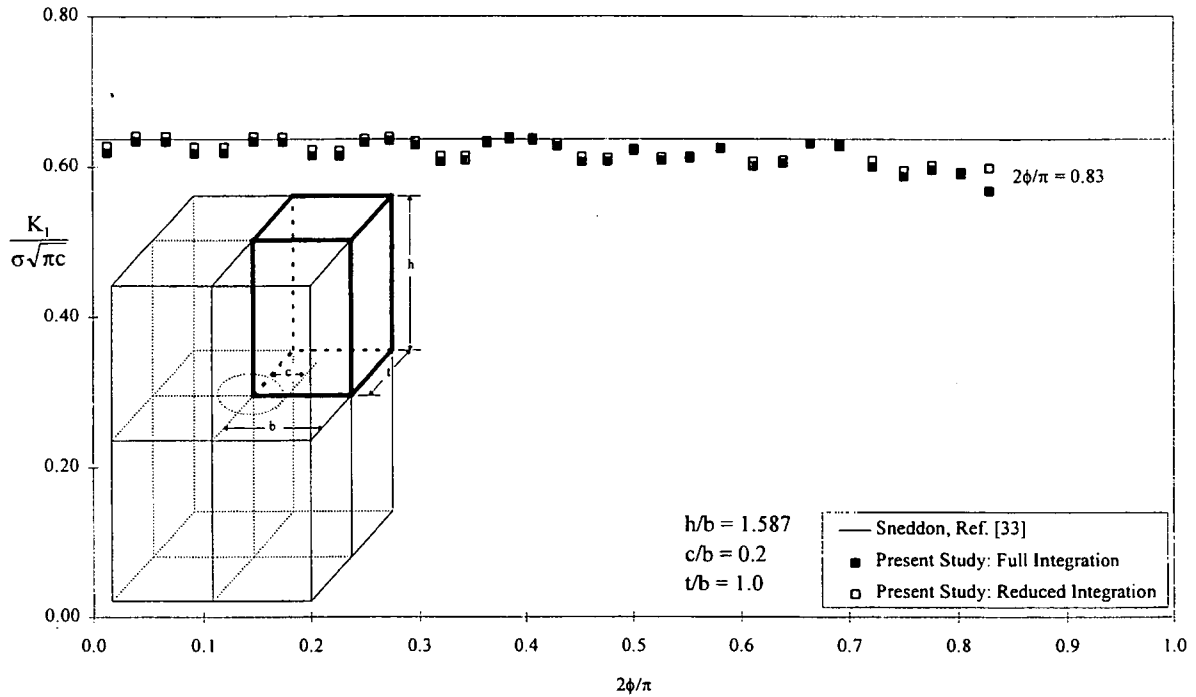


Figure 13 Comparison of Theoretical and FEA Solutions for Circular Internal Crack Embedded in an Infinite Solid Subject to Uniform Tension

Furthermore, at $\phi = 0$, the mesh is not skewed which indicates the element sides on the crack front are smaller than those at larger ϕ resulting in a better representation of the circular crack. Also at this location, the crack is furthest away from the boundaries of the plate mitigating any disruption of the stress field due to the boundary better representing an infinite solid. The deviation in the two solutions as ϕ approaches maximum is due to extremely skewed elements where the crack front is no longer circular since enforcing a circular boundary at this location would require collapsing the brick elements. Figure 11 illustrates the “flattening” of the circular crack at maximum ϕ . In addition, a slight difference in the analyses using full and reduced integration is also evident which is further indication the mesh is coarse. Reduced integration eliminates the displacements ultimately used to obtain the transverse shear stress in the global stiffness matrix of a finite element model. In doing so, the arbitrary stiffness associated with these shear stress is eliminated making the model more flexible. For fine mesh finite element models subject to tension only, full and reduced integration solutions should be coincident. A coarse mesh is arbitrarily stiff due to a lack of degrees of freedom. By using reduced integration on a coarse mesh, the stiffness associated with the available degrees of freedom decreases

making the model more flexible. As mentioned previously, reduced integration is only beneficial for bending dominant problems.

4.3 Cracks in Three Dimensional Finite Bodies

In attempts to better represent the physics of cracks occurring in operational structures, developing three dimensional stress intensity solutions has received much attention. In addition, the advances in computer technology have made possible solution of problems once too time consuming and cumbersome to generate. Recall the main goal of this effort is to generate three dimensional solutions for a semi-elliptical crack which has penetrated the back surface. Since there are limited solutions in which to compare the present results, verification of the methodology is done by generating K 's for known solutions. The following five sections present comparisons to center crack tension (CCT), single edge crack tension (SECT), semi-elliptical surface crack subject to tension and bending, diametrically opposed quarter elliptical corner crack at a hole subject to tension and bending, and center crack tension with a skewed mesh at the crack front.

4.3.1 Center Crack Tension

Three dimensional solutions for this and the following crack geometry, in addition to several other commonly used fracture specimens, were first generated by Raju and Newman in 1977 using the finite element method with singularity elements and the finite element method employing the force method.⁹ The model generated in our study contained 16112 elements, 18972 nodes, and 56,916 degrees of freedom; nearly 75 times more degrees of freedom than [9]. The increased refinement of the mesh is done to allow use of one mesh to generate multiple solutions, where in [9] each model was used for only one solution. Furthermore in [9], the mesh pattern surrounding the crack front is orthogonal to the crack front. Figure 14 presents the results from [9] and the present study. Excluding the boundary layer, correlation is good throughout the thickness of the model. The slight variation at the mid-plane is due to differences in the model height to width ratio, h/b , which is known to effect the stress distribution in the model.⁹ This St. Venant's behavior is accentuated as h/b decreases because the crack plane becomes closer to the point of load application. This height effect typically causes variations of one percent or less for h/b ratios in this range.³⁴ The height effect is small in the CCT models and can be ignored for $h/b \geq 2.0$. Near the peak K value in the boundary layer, the 0.67% difference is attributed to the current model having more degrees of freedom; thereby being more flexible resulting in a slightly higher K .

4.3.2 Single Edge Crack Tension

In reference [9] and the current study, the same model used for the CCT analysis is used for the Single Edge Crack Tension by simply removing the $u = 0$ at $x = 0$ boundary conditions which in the CCT analysis are used for creating the symmetry

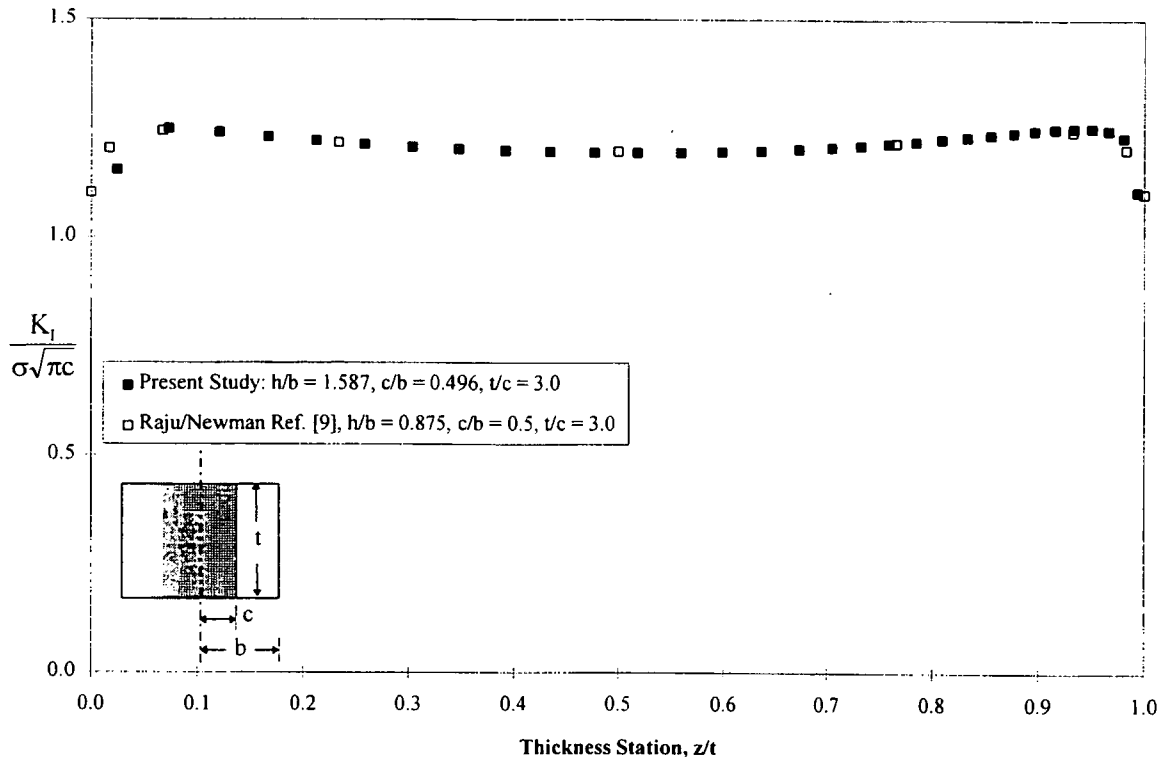


Figure 14 Comparison of CCT FEM Mode I Stress Intensity Factor Solutions

plane. A unit stress was applied at $y = h$ and no bending restrictions were enforced. Figure 15 shows the comparison between [9] and the present results. The 1.1% error evident through most of the cross section can only be attributed to the increased degrees of freedom in the present model. The height effect is extremely small in the SECT models and can be ignored for $h/b \geq 1.5$. The results of the two h/b values used in [9] are coincident.

4.3.3 Semi-Elliptical Surface Crack Subject to Tension and Bending

The model used to generate the circular internal crack embedded in an infinite solid (penny crack) is also used for the semi-elliptical surface crack subject to tension and bending by changing the boundary conditions. Recall symmetry boundary conditions are applied to reduce the size of the model.^{26,27,28,29} For the penny crack, symmetry planes lie at $x = 0$, $y = 0$, and $z = 0$ with sufficient explicit modeling in each of the positive axis directions to represent an infinite body. By removing the $w = 0$ constraint at $z = 0$, the penny crack model now represents a surface crack. The Newman/Raju solutions have become a standard of comparison for new K solutions of semi-elliptical cracks.³⁵ The Newman/Raju results shown in Figure 16 are derived from the equations presented in [35] not directly from the FEA results. As expected,

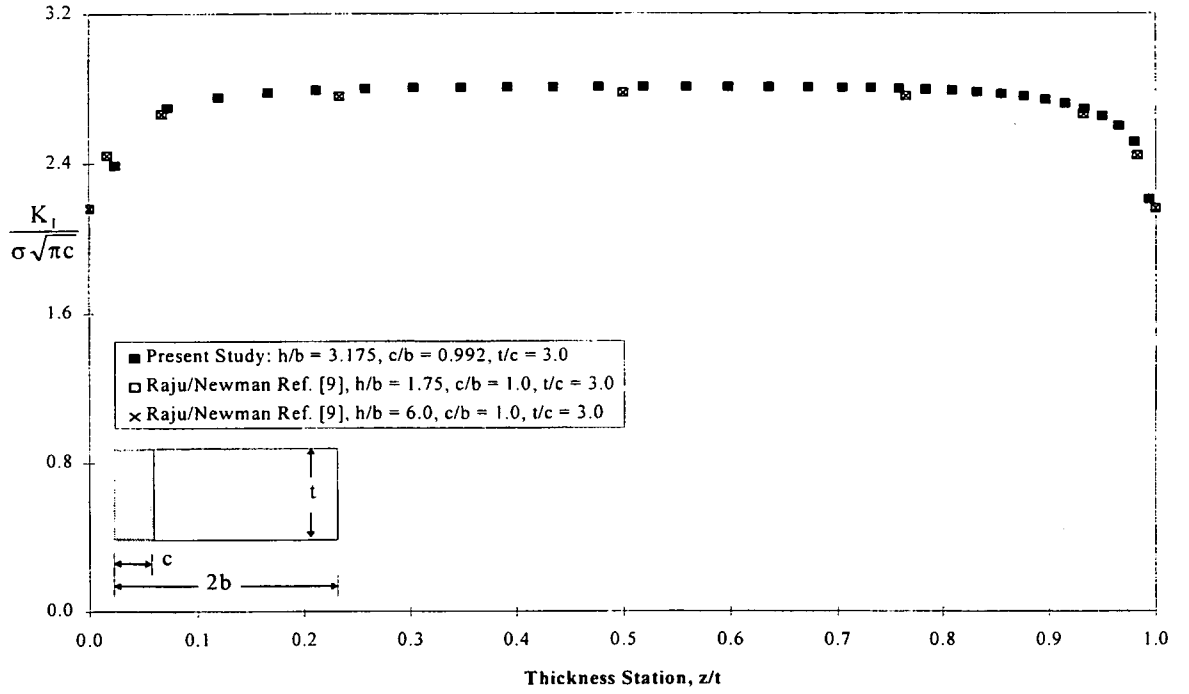


Figure 15 Comparison of SECT FEM Mode I Stress Intensity Factor Solutions

the general trend of the present analysis correlates well to the referenced solution, since this model is a derivative of the penny crack model, see the penny crack discussion for the explanation of the variation in solutions. Also recall, the back surface of the penny crack, and thus for the surface crack also, had to be flattened in order to prevent the elements from being extremely skewed which can lead to a singular stiffness matrix in the FEA.

The mode I stress intensity factor for cracks of a semi-elliptical form is normalized in the following manner.

$$\beta = \frac{K}{\sigma \sqrt{\pi a}} \quad (27)$$

$$\text{where } Q = 1 + 1.464 \left(\frac{a}{c} \right)^{1.65} \quad \text{for } \frac{a}{c} \leq 1.0$$

$$Q = 1 + 1.464 \left(\frac{c}{a} \right)^{1.65} \quad \text{for } \frac{a}{c} > 1.0 \quad (28)$$

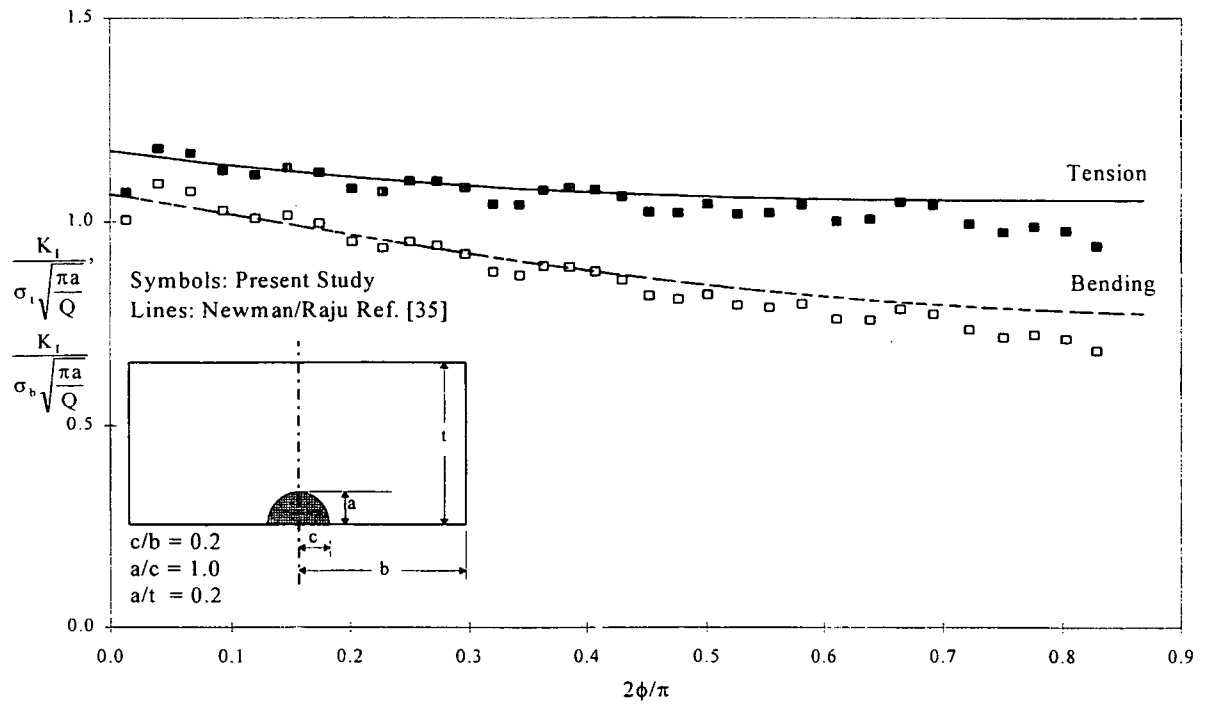


Figure 16 Comparison of Semi-Elliptical Surface Crack Subject to Tension and Bending FEM Mode I Stress Intensity Factor Solutions

The flaw shape parameter, Q as given by Eqn. (28), was derived by Rawe as an approximation to the square of the complete elliptical integral of the second kind which is required to represent the stress distribution around an elliptical crack in an infinite body.³⁶ Newman and Raju found the maximum error in the stress intensity factor by using these approximations is about 0.13% for all a/c values.³⁵ Subsequently, Schijve derived a more accurate solution to the complete elliptical integral, Φ :³⁷

$$\Phi = \frac{\pi}{2(1+m)} \left[1 + \frac{m^2}{4} + \frac{m^4}{64} \right] \quad (29)$$

$$\text{where } m = \frac{1 - \frac{a}{c}}{1 + \frac{a}{c}}$$

With Eqn. (29), the normalized mode I stress intensity factor can accurately be represented by the following equation.

$$\beta = \frac{K(\phi)}{\frac{\sigma \sqrt{\pi a}}{\Phi}} \quad (30)$$

4.3.4 Diametrically Opposed Through Cracks at a Hole Subject to Remote Biaxial Tension, Remote Bending, and Uniform Internal Pressure

In searching the literature, few stress intensity solutions exist for this crack geometry and load conditions. The solutions that are available are two dimensional only, and the Tweed/Rooke and NASGRO TC09 solutions are for an infinite plate; thus, finite width corrections are applied. The Newman and NASGRO TC09 solutions are nearly coincident varying by less than 1% for all crack lengths shown in Figure 17. The Tweed/Rooke solution differs by less than 0.5% for the smallest crack length; however, the difference increases with crack length to more than 9% for the largest crack length in Figure 17 when compared to Newman and NASGRO TC09.^{38,39,44} The correlation is satisfactory with the Newman and NASGRO TC09 solutions varying by less than 3.0% on average with the current 3D FEA results except for the smallest crack length where the mesh refinement in the crack wake of the current study is insufficient.

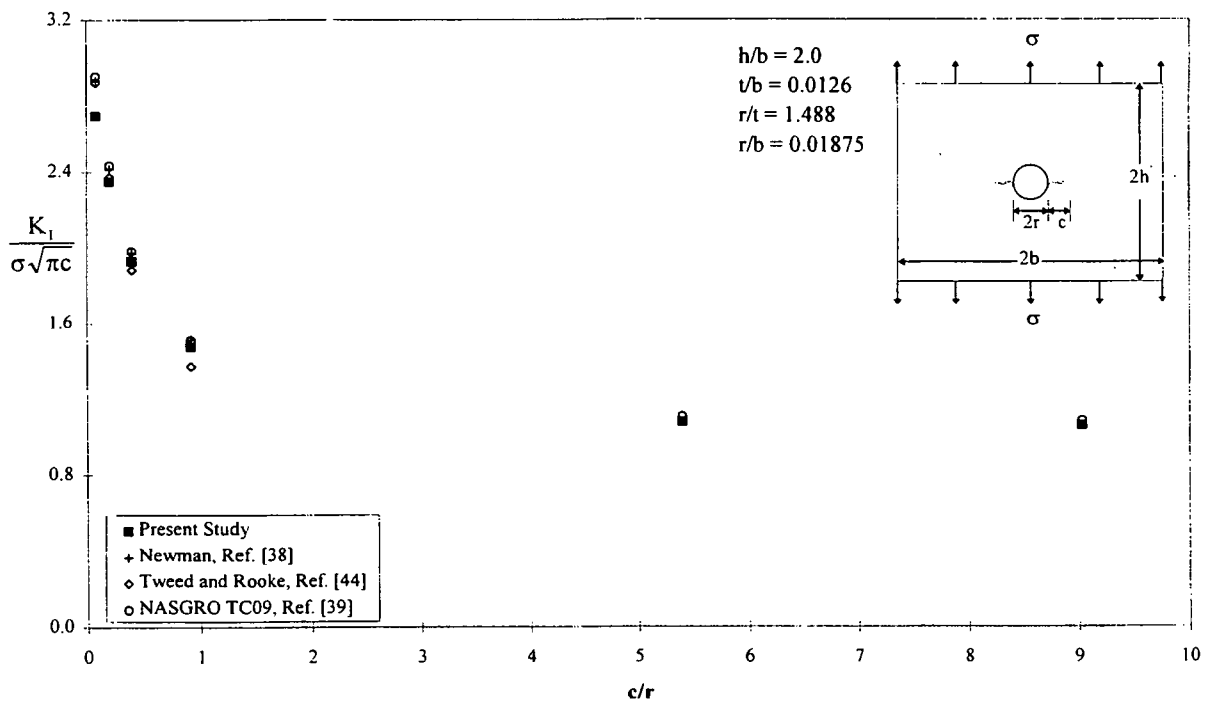


Figure 17 Comparison of Diametrically Opposed Through Cracks at a Hole Subject to Tension

The biaxial tension, uniform tension applied along all four plate edges, also correlates well with references [38] and [39] as shown in Figure 18. References [38] and [39] differ by 3.1% or less for all cracks lengths shown below. The maximum difference with the current 3D FEA results occurs at the smallest crack length which is again due to insufficient mesh refinement in the crack wake.

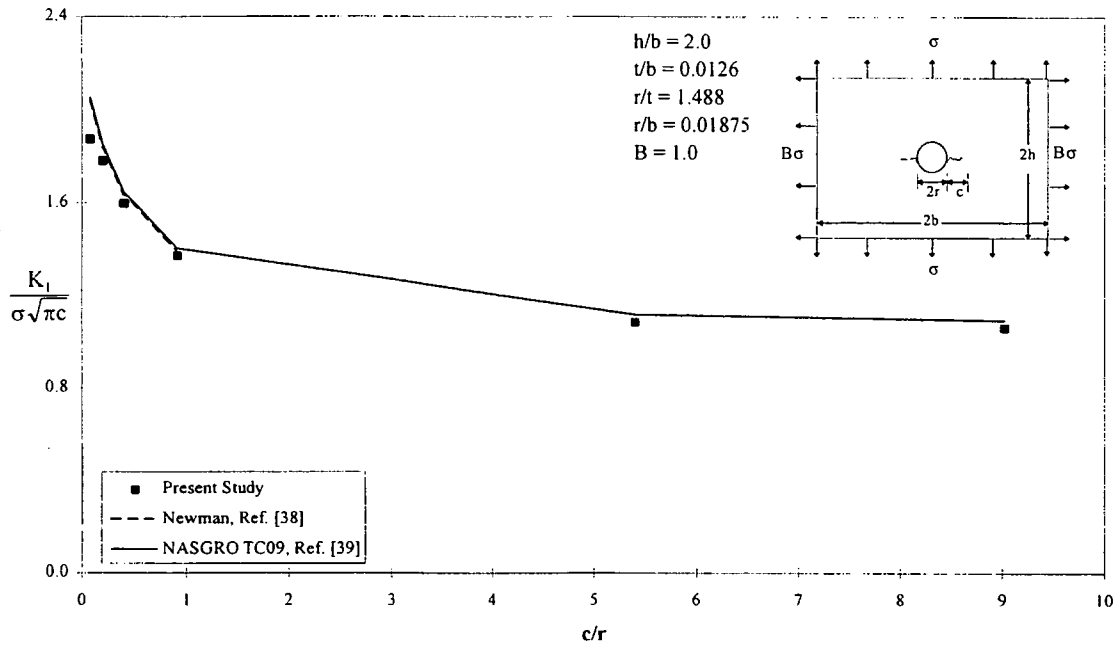


Figure 18 Comparison of Diametrically Opposed Through Cracks at a Hole Subject to Uniform Biaxial Tension

Only two solutions for comparison were available for this geometry subject to remote bending as shown in Figure 19. The linear distribution of K through the thickness for the 2D solutions is assumed for comparison with the present 3D solution. Good correlation is seen with the NASGRO TC09 solution which was derived using conformal mapping by several authors.^{39,40,41,42,43} Other than the solution being two dimensional, it is difficult to discern why the Tweed and Rooke solution is 23% lower than the present results.⁴⁴

A uniform internal pressure on bore of the hole only, not on the crack faces, is used extensively for the rivet loading analyses that are done later; therefore, a validation analysis is completed. Again, no three dimensional solutions exist, thus the comparison is with a two dimensional boundary collocation solution shown in Figure 20. The difference between the present plane strain analysis and reference [38] varies with the maximum being 3.2%.

By modifying the distribution of the internal pressure, point, cosine and cosine squared rivet load distributions are obtained when superposed with the remote tension as will be derived later.

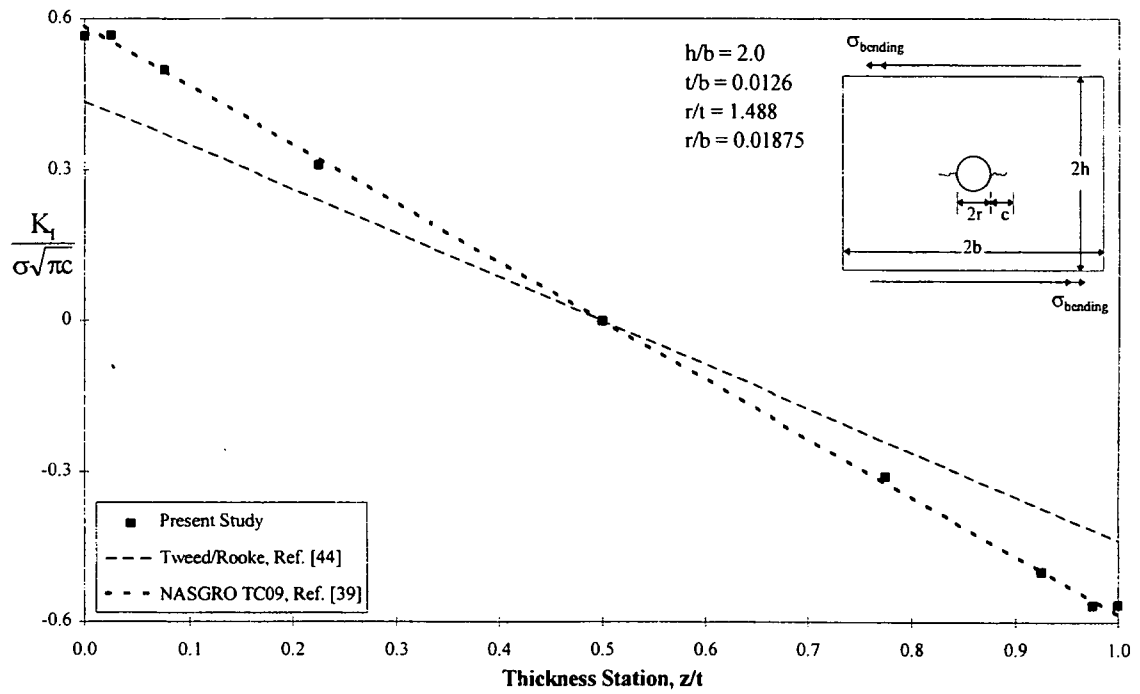


Figure 19 Comparison of Diametrically Opposed Through Cracks at a Hole Subject to Bending

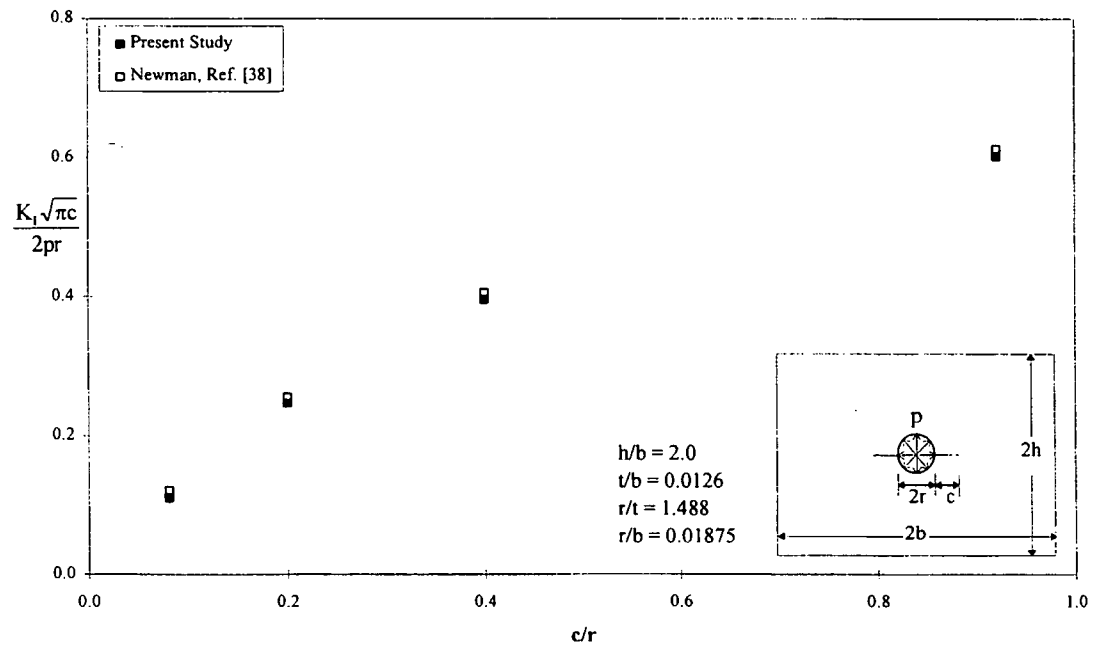


Figure 20 Comparison of Finite Width Plate with a Centrally Located Hole Subject to Uniform Internal Pressure

4.3.5 Through Cracks with an Oblique Elliptical Crack Front Subject to Remote Tension and Bending

The final verification models were designed to investigate the K variation along a through crack front since this will be of prime interest in future studies. Miyoshi et al. are the only researchers who have developed a solution for this geometry and load condition.^{45,46,47} They used the boundary element method to generate their solutions for varying a/t and a/c ratios. The accuracy of these solutions is “undefined.”⁴⁵ The model used for the straight through crack analyses was also used for this configuration by transforming the mesh to a part elliptical pattern as seen in Figure 21. The newly skewed mesh does not affect the K solutions as shown in the previous section. Figure 22 shows the good correlation found for the tension case. The solutions of references [46] and [47] do not account for the boundary layer effect; whereas, the present results do show the K drop off at the free surface where $\phi = 0$. Little variation in magnitude of either solution is evident through most of the plate thickness. As the point of back surface penetration is reached, the ligament between the crack front and back free surface is at a minimum elevating the stress field resulting in a sharp increase in K . Two other comparisons of the Miyoshi et al. solution were made yielding similar results, but are not shown here for brevity.

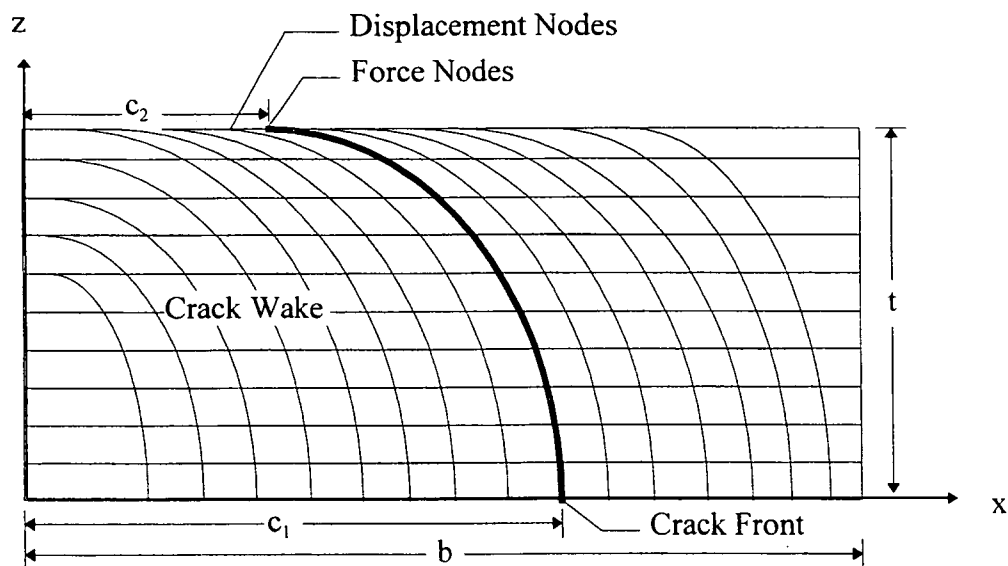


Figure 21 Diagram of Through Crack with Oblique Elliptical Crack Front

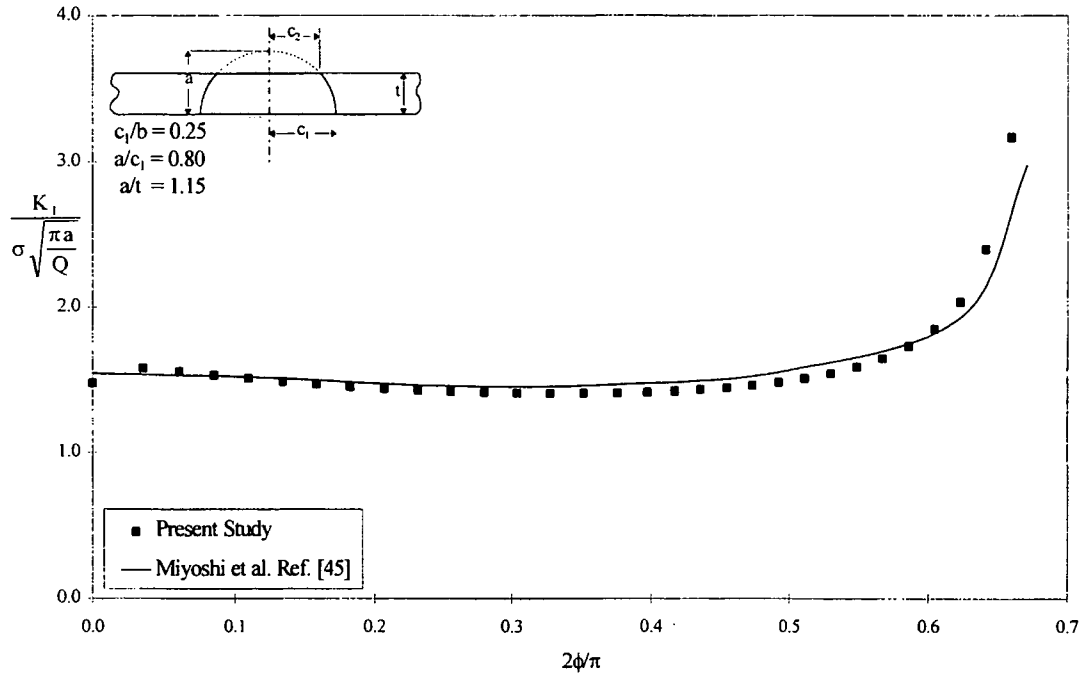


Figure 22 Comparison of Through Cracks with Oblique Elliptical Crack Front Subject to Remote Tension

The bending solution comparison is shown in Figure 23 for the same crack configuration as Figure 22.

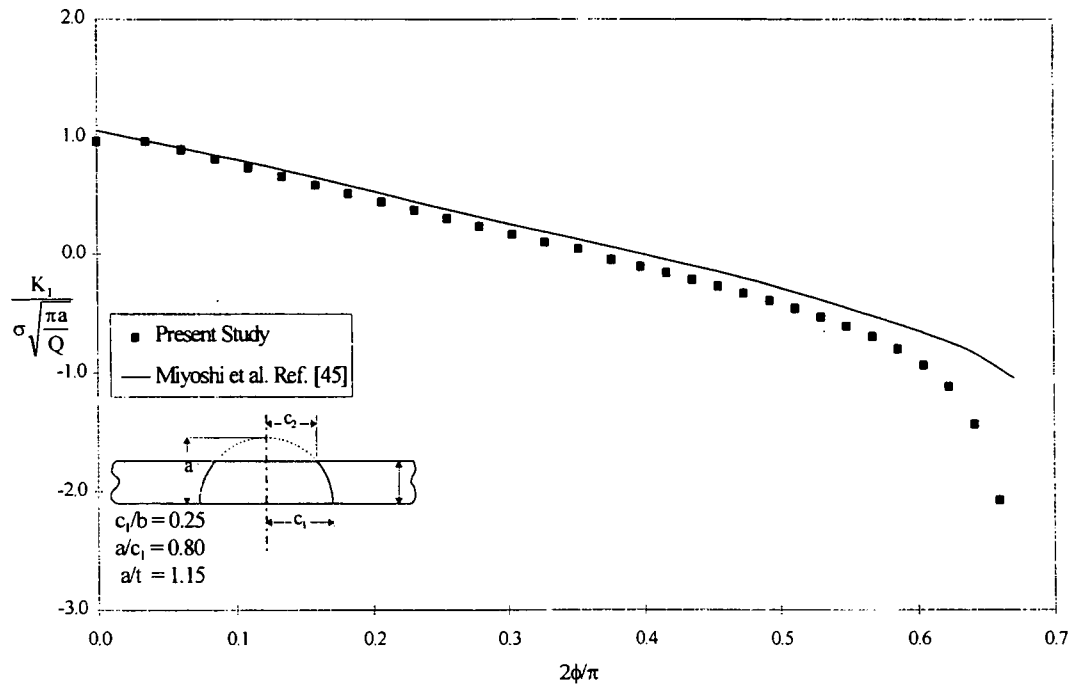


Figure 23 Comparison of Through Cracks with Oblique Elliptical Crack Front Subject to Remote Bending

Excellent correlation is seen at the free surface which is to be expected since the front free surface value should be invariant to the solution method. The Miyoshi et al. results show the transition from positive to negative K 's at $2\phi/\pi = 0.41$ ($z/t = 0.69$), whereas, the straight through crack subject to bending presented earlier transitioned at $z/t = 0.5$. Also note, the linear relationship is maintained until close to back surface penetration. The current results transition from positive to negative K 's at $2\phi/\pi = 0.375$ ($z/t = 0.64$) and show a stronger dependence on crack shape. A steeper linear variation is visible through $2\phi/\pi = 0.5$, and a more pronounced non linear gradient is apparent approaching back surface penetration.

Combining the tension and bending results shows the variation in K 's toward the back surface of the plate is additive, see Figure 24. However, the front surface K 's still exhibit excellent agreement. Since representing the crack boundary at the back surface is quite difficult researchers may be forced to use approximations in this area. The Miyoshi et al. results for the pre-penetrated cracks are simply semi-elliptical surface cracks for which various solutions are available. By comparing the surface crack K 's under remote tension and bending obtained by Miyoshi et al. to the Raju/Newman equations, shown in Figure 25, the dependence of K on the solution method is evaluated.³⁵ Recall, Miyoshi et al. used the boundary element method and Raju/Newman used the finite element method. The good agreement in the two surface crack solutions in Figure 25 indicate, as expected, the solution method has no effect on the stress intensity factor. Therefore, the differences between the current work and Miyoshi et al. is possibly due to modeling the crack boundary.

The post penetration bending results of Miyoshi et al. remain in question. Examining the tabular data in reference [45] for the bending case several trends are evident with respect to the normalized K ; for constant a/c , K increases with increasing a/t for all values of $2\phi/\pi$ which is expected since increases in a/t indicate an increase in the crack area. Furthermore, in the limit as a/t becomes infinite, the crack is no longer oblique but straight; therefore, the penetrated surface K 's should be of equal magnitude but opposite sign to the front surface K 's.

4.4 Influence of a Non Orthogonal Finite Element Mesh on Stress Intensity Factors Calculated Using the 3D VCCT.

Two final investigations are completed to further verify using the 3D VCCT and a non orthogonal, skewed, finite element mesh. Recall, the force and COD methods require an orthogonal mesh with respect to the crack front in order to obtain accurate SIF solutions. The 3D VCCT makes no restrictions. The following two analyses aim to illustrate the effect of a skewed mesh on K . The first is a straight through crack that has been arbitrarily skewed, the second, a mesh that may occur in calculating K 's for part-elliptical through cracks.

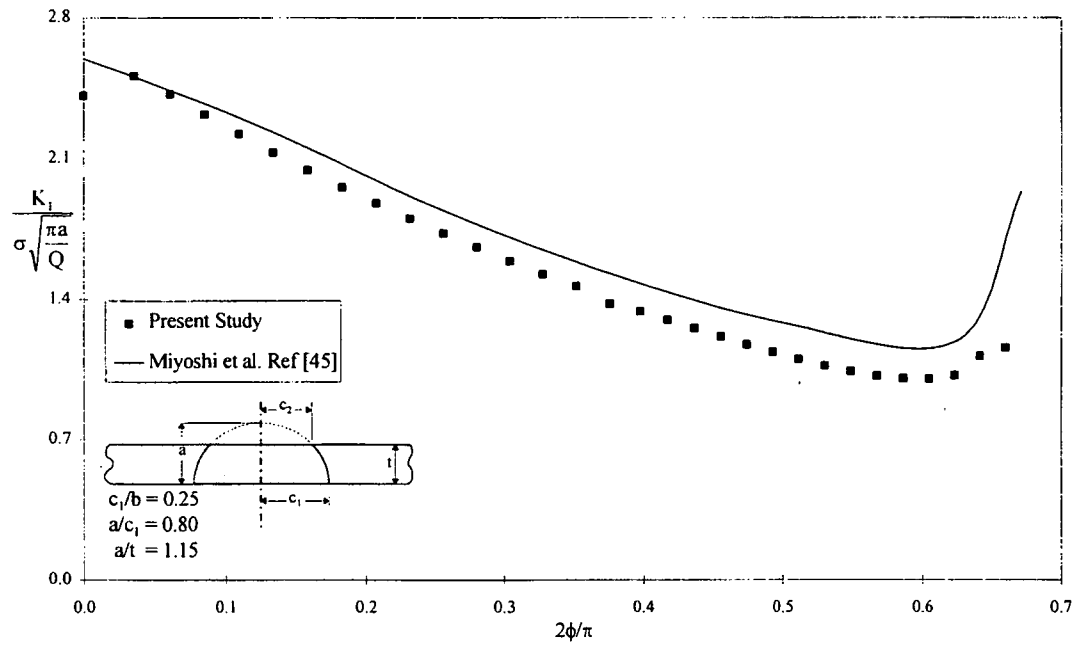


Figure 24 Comparison of Through Cracks with Oblique Elliptical Crack Front Subject to Remote Tension and Bending

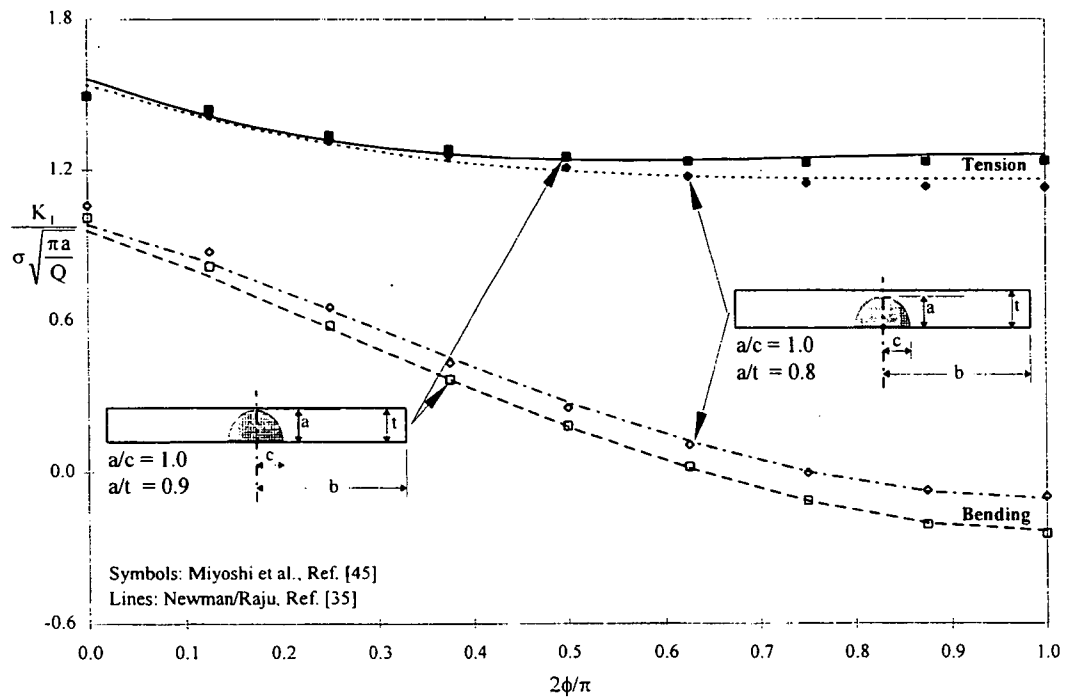


Figure 25 Comparison of SIF Solutions for a Semi-Elliptical Surface Crack Subject to Remote Tension and Bending

4.4.1 Center Cracked Tension with Skewed Mesh at the Crack Front Subject to Remote Tension

Using the straight through crack model described above, several orthogonal and skewed meshes were analyzed to see the effect of the non orthogonal mesh. The mesh around the crack front was skewed two different ways by translating in the thickness direction (z-direction) only. First, the nodes in the crack wake, one element behind the crack front, were linearly scaled by increasing the z coordinate by one half the original z dimension of the particular element. Then the nodes one element ahead of the crack front were linearly scaled by decreasing the z coordinate by one half the original z dimension of the particular element. The nodes one element behind, on, and one element ahead of the crack front now form a chevron as shown in Figure 26

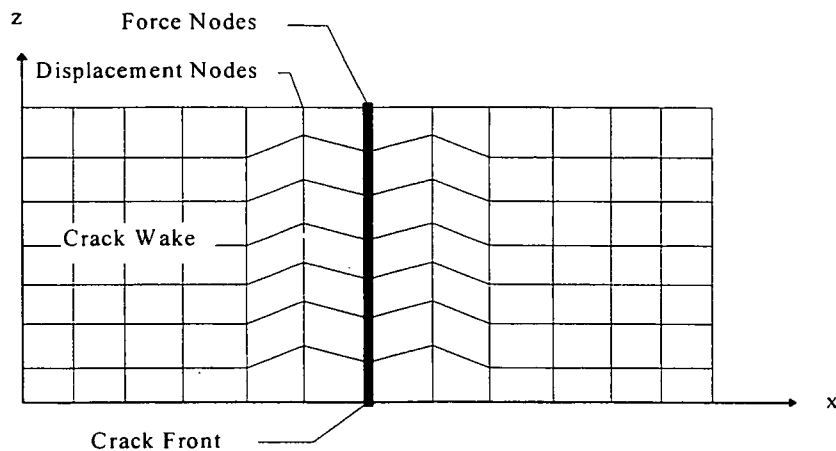


Figure 26 Diagram of Crack Plane of Chevron Skew Mesh with the Force and Displacement Nodes Used to Calculate K

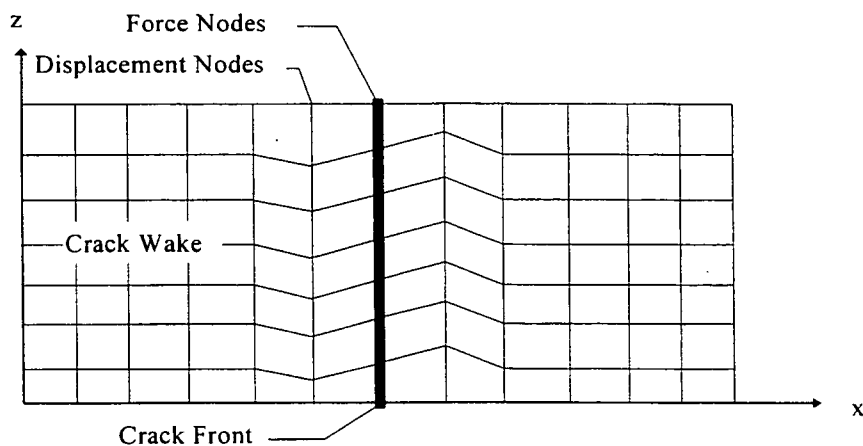


Figure 27 Diagram of Crack Plane of Linear Skew Mesh with the Force and Displacement Nodes Used to Calculate K

The second method of skewing the mesh uses the same process in the crack wake, but for the nodes one element ahead of the crack, the nodes are translated by increasing the z coordinate by one half the original z dimension of the particular element. The

nodes one element behind, on, and one element ahead of the crack front now form collinear parallelograms as shown in Figure 27. The analysis results for these two models are shown in Figure 28.

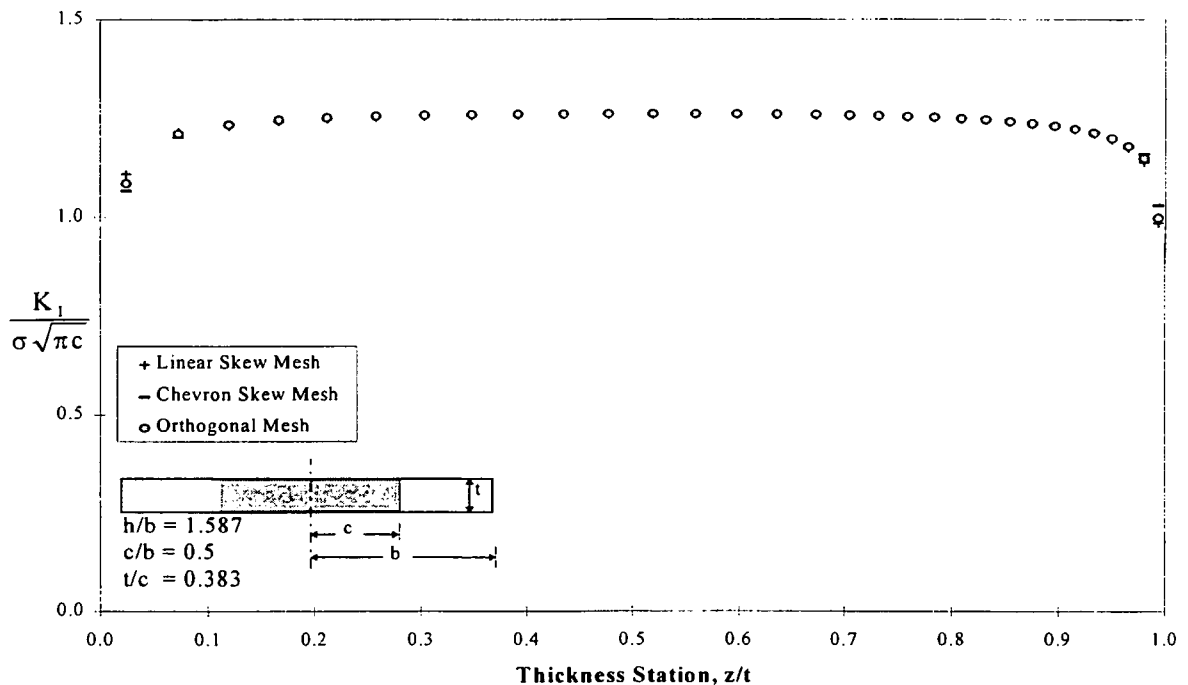


Figure 28 Effect of Mesh Pattern on the Mode I Stress Intensity Factor Solution for a Straight Through Crack Subject to Remote Tension

The small variation present is nearly uniform through the thickness; therefore, the mid plane K 's, $z = t/2$, are used for comparison. The difference is 0.14% for the Linear Skew Mesh and 0.008% for the Chevron Skew Mesh. From a geometric standpoint having a non orthogonal mesh for a straight through crack with equal element area behind and in front of the crack front is a difficult task without changing the global dimensions of the plate being modeled. As a result, for both skewed meshes, the elements at the boundary, $z = 0$ and $z = t$, have different areas than the interior elements. At the boundary, the unequal area elements are symmetric for the Chevron Skew Mesh and asymmetric for the Linear Skew Mesh. The 0.14% error for the Linear Skew Mesh is attributable to the asymmetry of the elements with respect to the crack front which is a requirement for the 3D VCCT. The 0.008% error for the Chevron Skew Mesh is due to the proximity of mesh transitions to the crack front which perturbs the local stress field thereby affecting the strain energy release rate calculations.

4.4.2 Internal Elliptical Crack Embedded in an Infinite Solid Subject to Remote Tension

For an elliptical crack front, a non orthogonal (skewed) mesh as shown in Figure 11 is quite easy to generate and modify. In addition, solution of this problem has been

addressed by other researchers which is useful for comparisons.^{48,49} The purpose of this analysis was to determine to what extent the elements could be skewed and still have negligible effect on the K's. The normalized skew ratio is defined as

$$NSR = \frac{90 - \alpha}{90} \quad (31)$$

where α is defined in Figure 29.

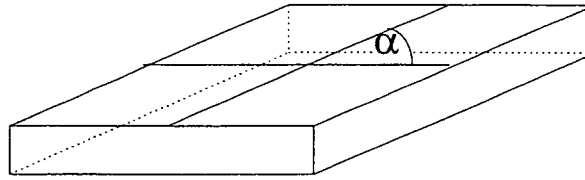


Figure 29 Definition of α

The normalized skew ratio for the elements approaching the minor axis of the ellipse was greater than 0.95 as seen in Figure 30. Skewing the elements any further results in a numerically unsolvable mesh. In other words, the integration points of the skewed elements are so close together, zero or negative volumes are calculated for them. Comparisons with known solutions are made in Figure 31. Even though the mesh is extremely skewed, the maximum error with respect to the Newman/Raju and Irwin solutions is 6%. Note, the Newman/Raju and Irwin solutions are coincident. The skew ratio of 0.95 is viewed as a limiting value.

In view of these present results, orthogonality of the mesh with respect to the crack front is not required for the 3D VCCT.

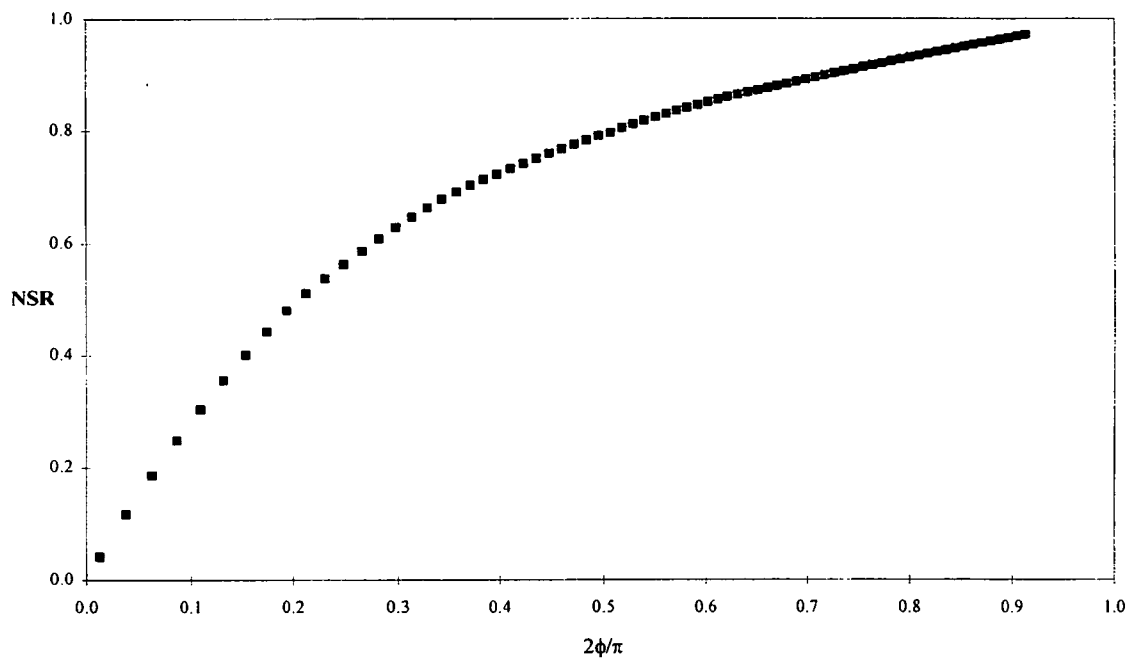


Figure 30 Normalized Skew Ratio for Finite Element Mesh of Internal Elliptical Crack Embedded in an Infinite Body

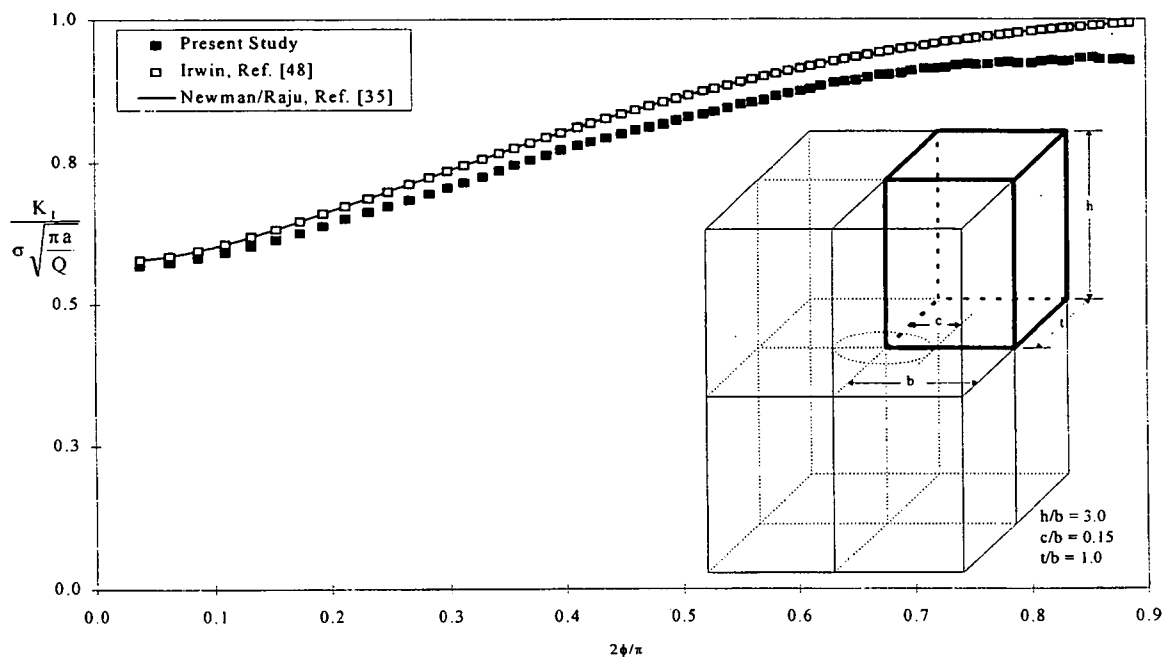


Figure 31 Comparison of Elliptical Internal Crack Embedded in an Infinite Solid Subject to Uniform Tension

5. Application Results

In the previous chapter the 3D VCCT was shown to provide accurate stress intensity factors for crack geometries and load conditions commonly found in riveted lap-splice joints in fuselages of transport aircraft. Now this technique is used to obtain a qualitative understanding of the influence of varying load conditions and crack geometries on the stress intensity factor; specifically, the degree of biaxiality, assumed rivet load distribution, and oblique crack fronts. These qualitative results are assumed to apply for the through cracks with oblique elliptical crack fronts which are the main focus of this research effort; however, the results for the latter will be reported in a future publication.

5.1 Diametrically Opposed Through Cracks at a Hole

Three dimensional finite element models for diametrically opposed through cracks at a hole in a finite width plate are developed and analyzed. Again, only one quarter of the plate is modeled due to the available symmetry planes. The only published solutions for this crack geometry are two dimensional and obtained via conformal mapping^{50,42,43} or boundary collocation.³⁸ In addition, referenced solutions are for infinite plates with only one crack; therefore, finite width^{51,52} and Shah⁵³ corrections are superposed in the literature.

5.1.1 Biaxial Tension

The published solutions, references [38], [39], and [51] for this load case vary less than 1% with respect to one another; therefore, only one solution is presented for comparison. Figure 32 shows the results for six crack lengths loaded by biaxial tension, biaxiality ratio, B , ranging from 0.0 - 1.0. The largest difference between reference [39] and the present results occurs for the smallest crack length where [39] overestimates K by 4.7%. The difference decreases with crack length, for the largest crack length [39] underestimates K by 2.4%.

Both published and present results show the influence of the biaxiality wanes with increasing crack length. For small cracks, $c/r < 1.0$, the K reduction due to biaxiality, $B = 0$ compared to $B = 1$, is approximately 32% which is near the theoretical value of 33% for a crack length approaching zero. Another interesting trend is evident in Figure 32 when comparing the effect of the biaxiality for small and large cracks. For the small cracks, K decreases with increasing B ; whereas for the larger cracks K slightly increases for increasing B . The behavior is due to the changing stress field with increasing c/r as can be seen in Figure 33.

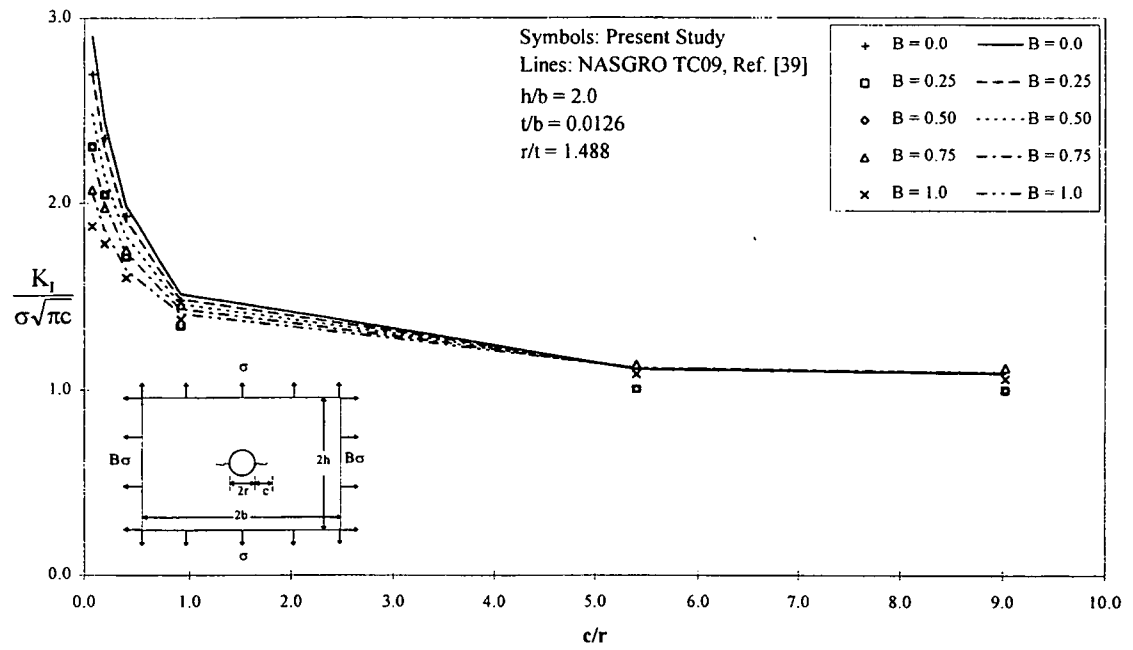


Figure 32 Comparison of Diametrically Opposed Straight Through Cracks from a Central Hole in a Finite Width Plate Subject to Varying Degrees of Biaxiality

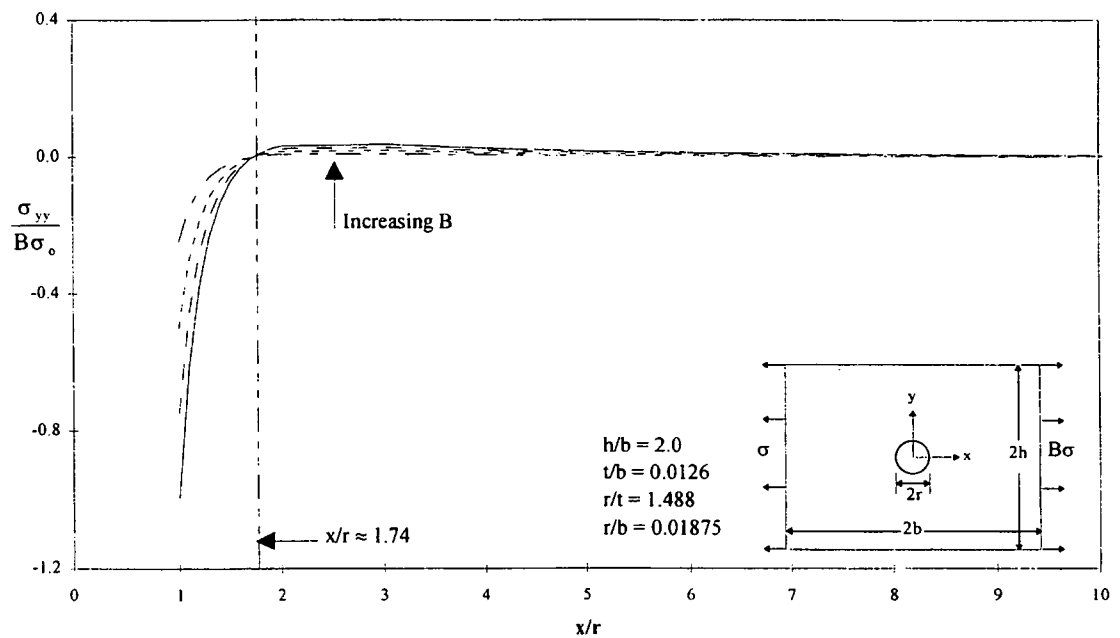


Figure 33 Crack Opening Mode Stress Due to Biaxial Loading

The crack opening mode stress, σ_{yy} , due to the biaxial loading is compressive from the hole edge to approximately three quarters of a hole radius away from the hole where it transitions to a tensile stress. The tensile stress beyond one hole radius from the hole edge result in the higher K values with increasing B seen in Figure 32. One final note on the effect of the biaxiality, the magnitude of the stresses in Figure 33 illustrates why the influence of the biaxial stress decreases with crack length.

5.1.2 Pin Loaded Hole

The same finite element model used in the previous section is also used to generate stress intensity factors due to the rivet loading. One of the fundamental issues to resolve in this part of the investigation is which load distribution to assume on the bore of the hole. Several researchers have addressed this question in developing stress concentration factors, K_t 's.^{54,55,56,57} Three different pin load distributions have been used in the literature; point, cosine and cosine squared loading. A parametric study has been accomplished to illustrate the effect of the pin load distribution on K. A priori, the point load results will be questionable since using point loads in a finite element model yields poor load introduction. This effect should be magnified for the smaller crack lengths where the point of load application is in close proximity to the crack front.

In order to make use of symmetry in a finite element model, the model must be symmetric with respect to geometry, load conditions, and material properties. Assuming the material is homogeneous and isotropic, a simple representation of a lap-splice joint, F in Figure 34, is geometrically symmetric but is not loaded symmetrically.

By decomposing F into components P and B, B is now symmetric but P must be further decomposed to obtain load symmetry. Case P is simply a pin loaded hole whereby the applied remote tensile stress is reacted entirely by the pin. Figure 35 illustrates the decomposition of P, which leads to:

$$K_P = K_B + K_D - K_E \quad (32)$$

In Figure 35, K_E is equal to K_P ; therefore Eqn. (32) implies

$$K_P = \frac{K_B + K_D}{2} \quad (33)$$

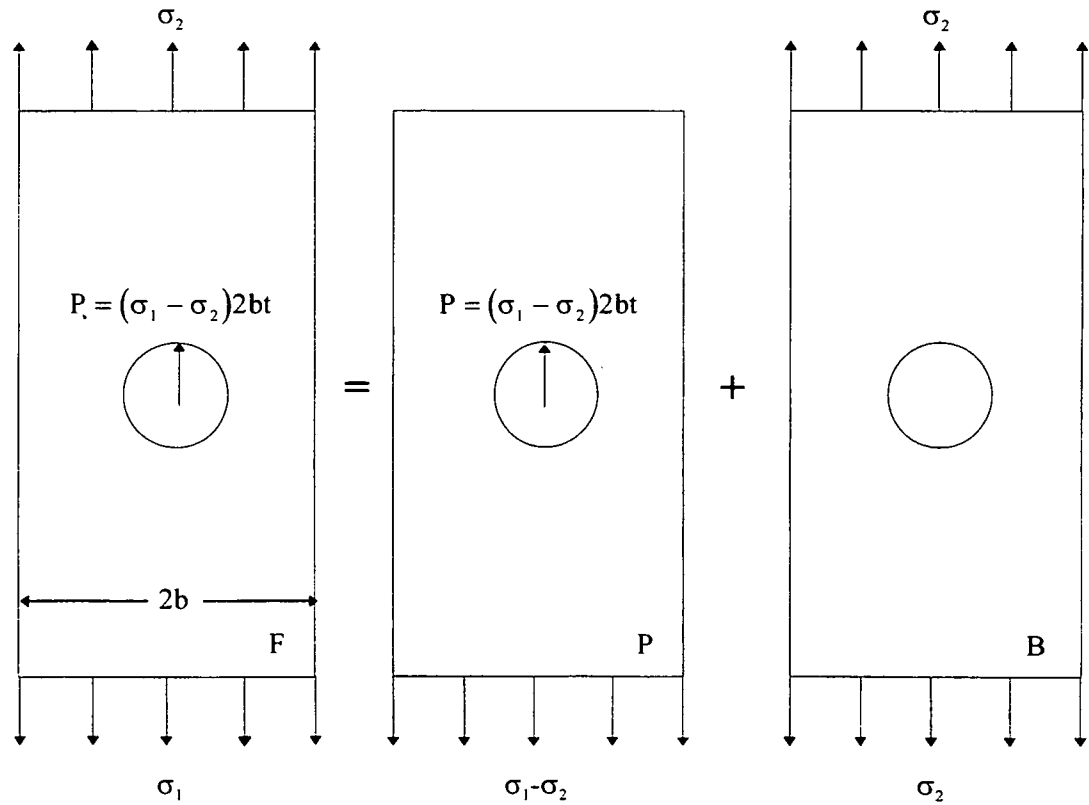


Figure 34 Decomposition of loads in typical single shear lap-splice joint

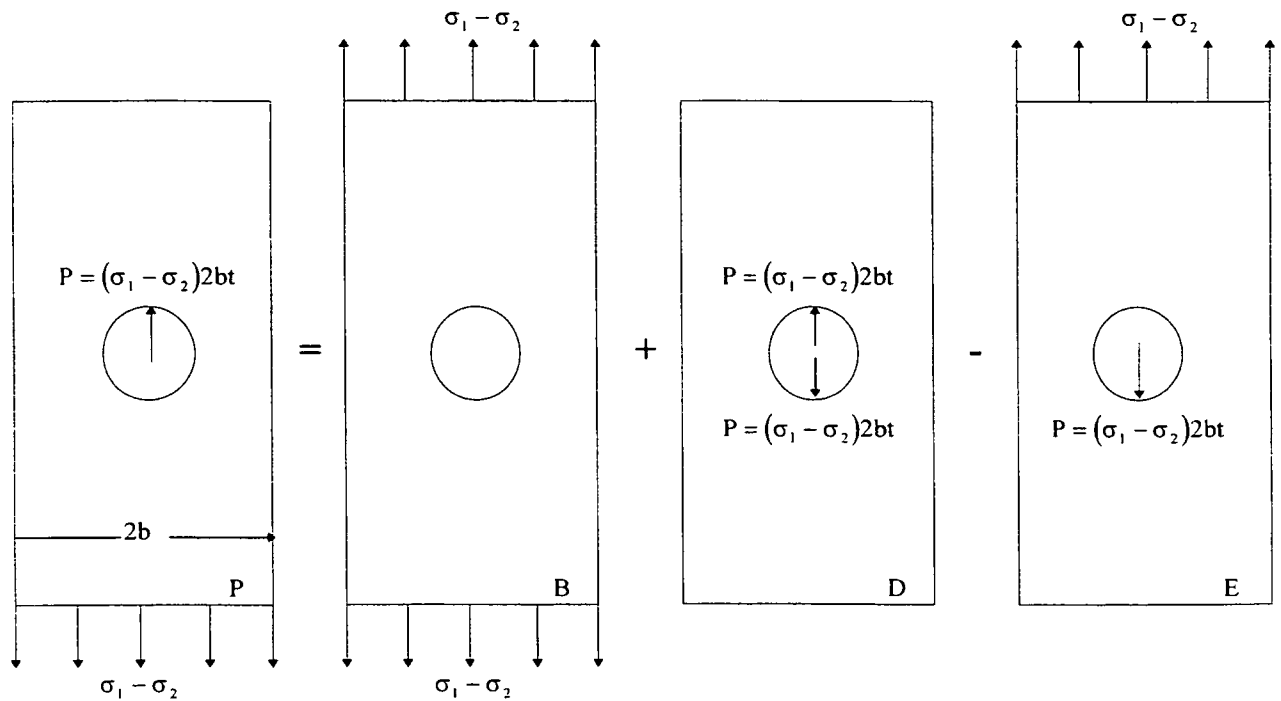


Figure 35 Decomposition of Pin Loaded Hole

Now for general applicability of this solution, it is more convenient to normalize K. The normalized K for each symmetric part is written as,

$$K_B = \sigma_T \sqrt{\pi a} \beta_T \quad (34)$$

where

$\sigma_T = \sigma_1 - \sigma_2$ Remote tensile stress

$\beta_T \equiv$ Boundary correction factor for finite width plate with central hole loaded by remote tension

and

$$K_D = \sigma_{Brg} \sqrt{\pi a} \beta_w \quad (35)$$

where

$\sigma_{Brg} \equiv$ Bearing stress

$\beta_w \equiv$ Boundary correction factor for finite width plate with central hole loaded by internal pressure (wedge loading)

Eqns. (34) and (35) are rewritten in terms of the load.

$$K_B = \frac{P}{2bt} \sqrt{\pi a} \beta_T \quad (36)$$

where

$$P = \sigma_T 2bt = (\sigma_1 - \sigma_2) 2bt$$

and

$$K_D = \frac{P}{2rt} \sqrt{\pi a} \beta_{Brg} \quad (37)$$

where

$$P = \sigma_{Brg} 2rt$$

Now combining Eqns. (33), (36) and (37),

$$K_P = \frac{\frac{P}{2bt} \sqrt{\pi a} \beta_T + \frac{P}{2rt} \sqrt{\pi a} \beta_{Brg}}{2} \quad (38)$$

Recall the normalization of K, in general can be written as

$$\beta = \frac{K}{\sigma\sqrt{\pi a}}$$

thus, the boundary correction factor for the pin load, β_p , is expressed as

$$\beta_p = \frac{\left(\frac{r}{b}\right)\beta_T + \beta_{Brg}}{2} \quad (39)$$

The r/b in Eqn. (39) is due to the correction factor for case B being normalized by the tensile stress and case D by the average bearing stress. Eqn. (39) is the most convenient form for derivation of K by the finite element method. In practice, for a 1/4 plate model of case P shown in Figure 35, two analyses must be run; one for remote tension and the other for the pin load.

5.1.2.1 Rivet Loading

Three different rivet load distributions were chosen to evaluate the effect of the rivet load distribution on K . Traditionally, the rivet load is modeled as a concentrated load located at the top of the hole, $\theta = 0^\circ$, but due to recent investigations on the stress concentration factor of a loaded hole a cosine or cosine squared distribution may be more appropriate.⁵⁴⁻⁵⁸ The effect of the assumed rivet load distribution is quite evident as seen in Figure 36 in addition to a comparison with reference [39]. The influence of the rivet load distribution is large for the small cracks and diminishes with increasing crack length. The cosine distribution gives the highest K for the smallest crack length due to the proximity of the applied load to the crack tip. This behavior can be easily explained by the K solution for a through crack in a finite width plate subject to eccentric concentrated loads on the crack face as shown in Figure 37 and in functional form by the following equation.

$$K_{IA} = \frac{P}{\sqrt{\pi c}} \sqrt{\frac{c+x}{c-x}} \quad (40)$$

As the point of application of load approaches the crack tip, the stress intensity increases sharply. Even though the magnitude of the applied load for both the cosine and cosine squared distributions approaches zero at the hole edge, the cosine distribution has a higher magnitude relative to the cosine squared; thus resulting in a higher K for the cosine distribution at the smallest crack length. The concentrated load being applied at the top of the hole, yields the smallest K for the smaller crack length.

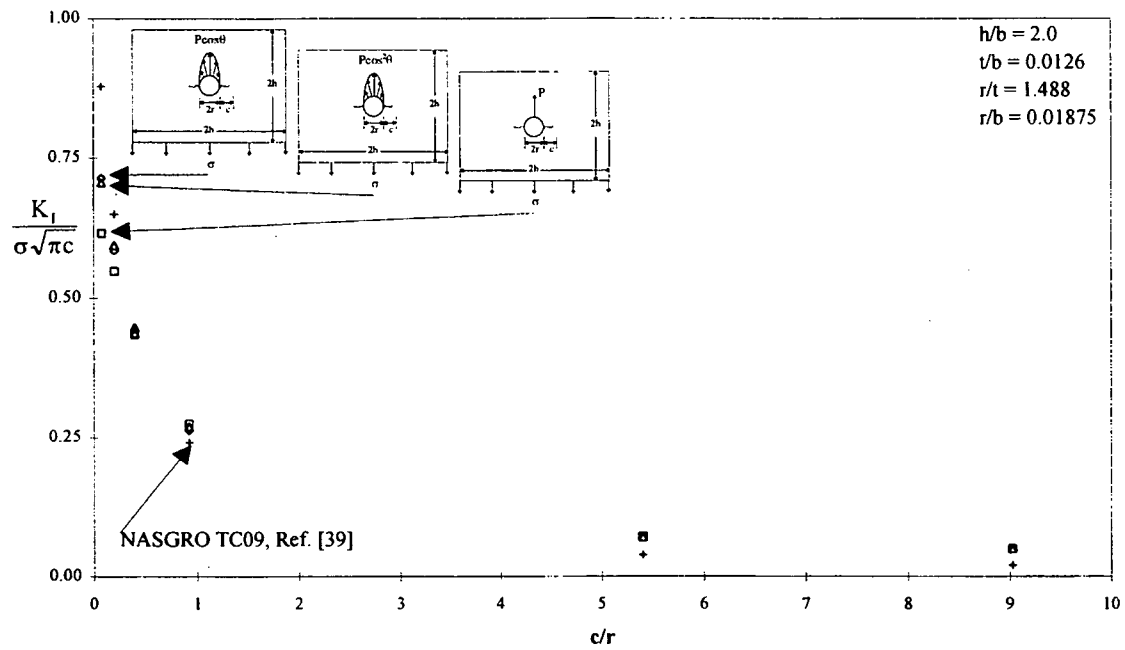


Figure 36 Effect of Rivet Load Distribution on Normalized K

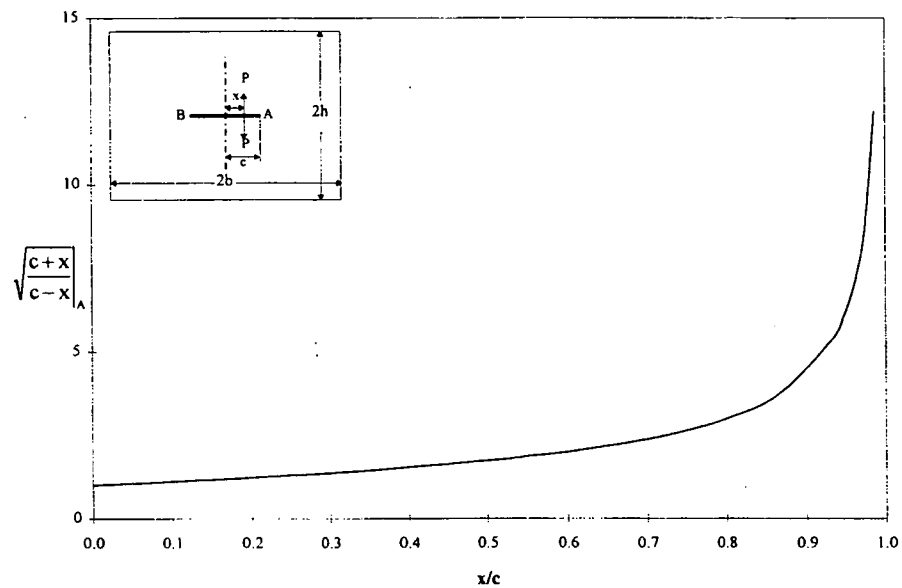


Figure 37 Effect of Load Location on Normalized K

A similar trend as in previous comparisons to reference [39] is apparent, over estimation of K for small cracks and very small underestimation of K for large cracks. Since the majority of the fatigue life occurs during crack nucleation and growth to a visible crack, using the reference [39] solution is conservative.

5.1.2.2 Rivet Tilting

In close cooperation with A. U. de Koning and C. Lof of the National Aerospace Laboratory of The Netherlands, cursory investigations are completed in an attempt to understand the effect of rivet tilting on K . The type of load distribution to assume due to rivet tilting is unknown and could not be found in the open literature. As can be expected, subtle changes in the assumed load distribution greatly effects the stress intensity factor. Therefore, this investigation is to be addressed in the future.

5.2 Effect of Oblique Crack Shape on Stress Intensity Factor

From an engineering point of view, accounting for the oblique shape through cracks with an oblique elliptical crack front is traditionally accomplished by assuming the oblique crack has a crack front perpendicular to the sheet surface and a crack length c_1 , recall definition of c_1 in Figure 21. This approach is undoubtedly conservative for those applications where the c_1 crack is visible. For riveted lap joints however, the visible crack is the penetrated crack, c_2 , and the c_1 crack, faying surface crack, length is unknown without disassembling the joint; an impractical solution for transport aircraft fuselage skin. Using the same model as in the previous section, a sensitive study is accomplished to determine the effect of the oblique shape. In Figure 39, a comparison is made between an oblique crack with an elliptical crack front ($a/c_1 = 0.56$) and two through cracks with straight crack fronts ($c = c_1$ and $c = c_2$, respectively). As seen in Figure 38, an oblique crack subject to remote tension can almost be regarded as a straight through crack when comparing the results of the 3D FEMs. Failure is dictated by the c_1 crack length; therefore, the higher K 's at the penetrated surface are of no consequence. If 3D solutions are not available, using the secant approximation, Eqn. (41), with c_1 yields an overestimation of K by 5% just inside the free surface, ignoring the boundary layer.

$$K_1 = \sigma \sqrt{\pi c} \sqrt{\sec\left(\frac{\pi c}{2b}\right)} \quad (41)$$

In the context of lap joints, the free surface is considered to be the surface where c_1 is measured. Using Eqn. (41) with c_2 results in an underestimation of K by 3.5%.

For remote tension, the higher K 's at the penetrated surface supports the catch-up behavior reported by Grandt et al. However, for the same configuration as Figure 38 when remote bending is applied catch-up of the penetrated crack is not likely as seen by Figure 39. The most striking result here is at the free surface where the 2D solution using $c_1 = c = 3.125$ underestimates K by 17.5% when subject to both tension and bending. Recall, the tension only analysis showed a 5% overestimation of K for this case. The 2D bending solution appears to be inadequate. The 3D FEM solution for the straight cracks both overestimate K at the free surface and could therefore be

used to approximate the oblique crack without the extra resources required to model the latter.

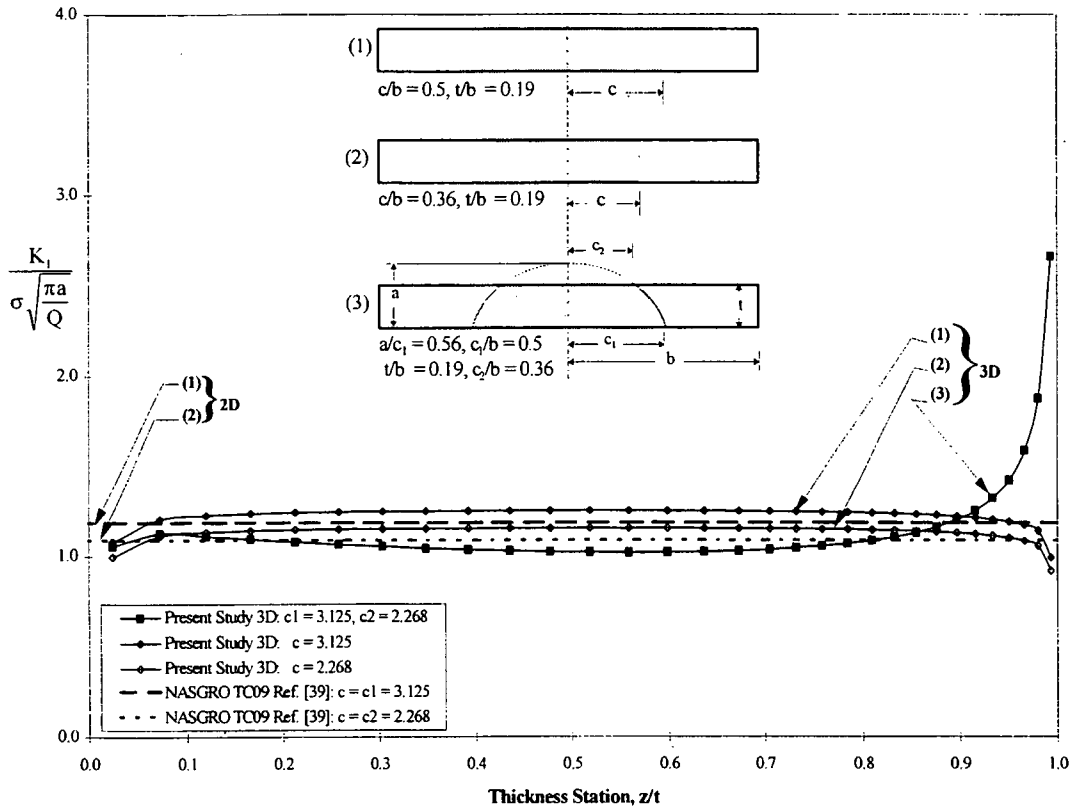


Figure 38 Sensitivity of K to Crack Shape Subject to Remote Tension

6. Conclusions

It has been shown that the 3D virtual crack closure technique (3D VCCT) can be used with a non orthogonal finite element mesh for the calculation of stress intensity factors. By generating one sufficiently fine finite element mesh, the 3D VCCT can be used to generate multiple stress intensity solutions of cracks with complex shapes by simply manipulating the crack plane geometry.

K solution results were calculated with 3D VCCT for crack configurations and loading cases for which results were available in the literature. The configurations covered were circular internal crack embedded in an infinite solid subject to uniform tension, center crack tension, single edge crack tension, diametrically opposed through cracks at a hole subject to tension, bending, biaxial tension, and pin loading, semi-elliptical surface crack subject to tension and bending, and through cracks with an oblique elliptical crack front subject to tension and bending. In general the agreement was within 5% when comparing to 2D analytical solutions and 1% when comparing to published 3D finite element solutions.

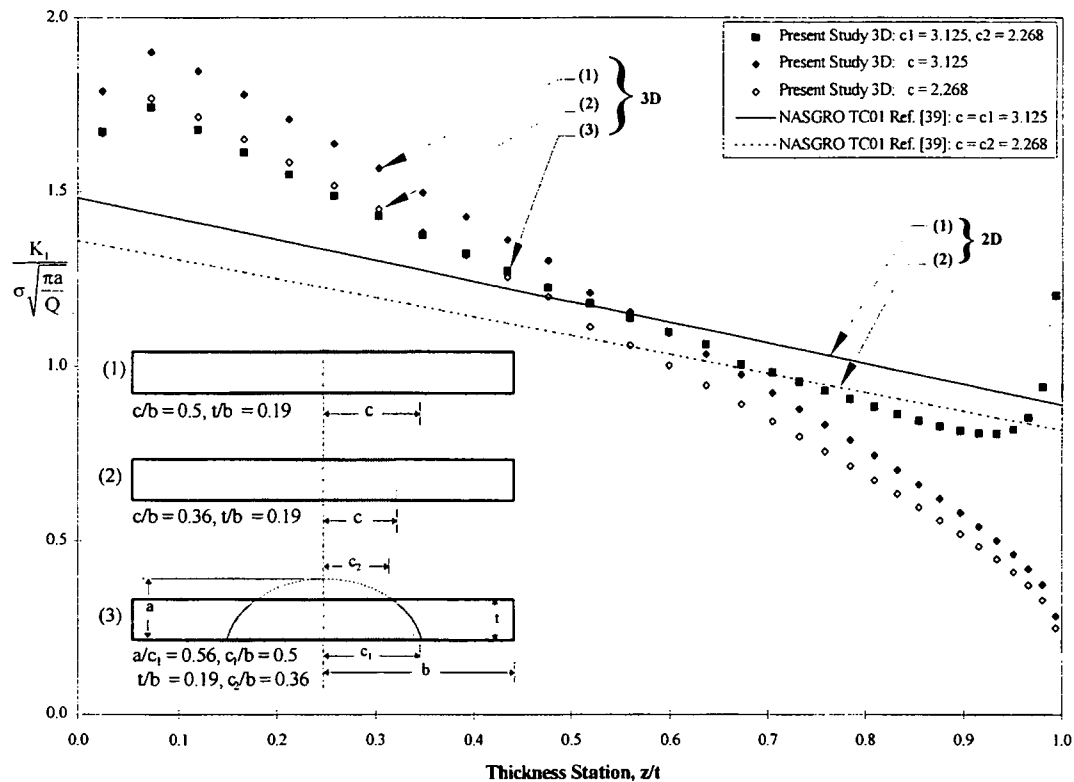


Figure 39 Sensitivity of K to Crack Shape Subject to Remote Tension and Bending

The effect of biaxial tensile loading on K for a finite width plate with diametrically opposed through cracks at a hole varies with crack length. For small cracks, ($c/r < 1.0$), increasing the biaxiality ratio decreases K ; whereas for larger cracks ($c/r \geq 1.0$), it locally increases K to a very small extent.

The assumed rivet load distribution on the bore of the rivet hole greatly influences K for small cracks, but has no measurable effect for large cracks. To remain conservative, a cosine squared distribution should be assumed unless the rivet load distribution is known.

K solutions were calculated for through cracks with an oblique elliptical crack front subject to tension and bending. For the tension case, the oblique crack can be approximated as a straight crack having a crack front perpendicular to the sheet surface and crack length equal to the largest crack length of the oblique crack which has penetrated a free surface. Also, the high K 's on the penetrated surface would promote catch-up where the penetrated crack grows rapidly to the same length as the free surface crack. For the bending case, however, the oblique crack cannot be approximated with a straight crack. No catch-up behavior seems possible since the K 's for the penetrated surface crack are lower than those of the faying surface.

A collaborative effort with the National Aerospace Laboratory of The Netherlands is underway to investigate the effect of rivet interference as a function of the rivet squeeze force and rivet tilting on the stress intensity factor.

7. References

- ¹ Müller, Richard Paul Gerhard, "An Experimental and Analytical Investigation on the Fatigue Behaviour of Fuselage Riveted Lap Joints, The Significance of the Rivet Squeeze Force, and a Comparison of 2024-T3 and Glare 3, Ph.D. Dissertation, Delft University of Technology, Faculty of Aerospace Engineering, Delft, The Netherlands, November 1995.
- ² Grandt, Jr., A. F., J. A. Harter, and B. J. Heath, "Transition of Part-Through Cracks at Holes into Through-the -Thickness Flaws," Fracture Mechanics: Fifteenth Symposium, ASTM STP 833, R. J. Sanford, Ed., American Society for Testing and Materials, Philadelphia, 1984, pp. 7-23.
- ³ Piascik, Robert S., Scott A. Willard, and Matthew Miller, "The Characterization of WideSpread Fatigue Damage in Fuselage Structure, " NASA Technical Memorandum 109142, Sep. 1994.
- ⁴ Jeong, D. Y., D. P. Roach, J. V. Canha, J. C. Brewer, and T. H. Flournoy, "Strain Fields in Boeing 737 Fuselage Lap Splices: Field and Laboratory Measurements with Analytical Correlations," DOT/FAA/CT-95/25(DOT-VNTSC-FAA-95-10), FAA Technical Center, Federal Aviation Administration, US Department of Transportation, Jun. 1995.
- ⁵ Bartelds, G. and A. U. de Koning, "Application of Finite Element Methods to the Analysis of Cracks, (Phase I - Evaluation of Methods)," National Aerospace Laboratory of The Netherlands, NLR TR 78138 U, Dec. 1987.
- ⁶ de Koning, A. U., Electronic Communication, The National Aerospace Laboratory of The Netherlands, 19 Jun. 1996.
- ⁷ de Koning, A. U., Personal Communication, The National Aerospace Laboratory of The Netherlands, 7 Jun. 1996.
- de Koning, A. U., Electronic Communication, The National Aerospace Laboratory of The Netherlands, 19 Jun. 1996.
- ⁸ Raju, I. S., J. C. Newman, Jr., "SURF3D: A 3-D Finite-Element Program for the Analysis of Surface and Corner Cracks in Solids Subjected to Mode-I Loadings," Technical Report NASA TM-107710, Feb. 1993.
- ⁹ Raju, I. S. and J. C. Newman, Jr., "Three-Dimensional Finite-Element Analysis of Finite-Thickness Fracture Specimens," Technical Note NASA TN D-8414, May 1977.
- ¹⁰ Dixon, J. R. And L. P. Pook, "Stress Intensity Factors Calculated Generally by the Finite-Element Technique," NATURE, Vol. 224, 1969, p. 166.
- ¹¹ Mowbray, D. F., "A Note of the Finite-Element Method in Linear Fracture Mechanics," Engineering Fracture Mechanics, Vol. 2, 1970, p. 173.

¹² Parks, D. M., "A Stiffness Derivative Finite Element Technique for Determination of Crack Tip Stress Intensity Factors," International Journal of Fracture, Vol. 10, No. 4, Dec. 1974.

¹³ Hellen, T. K., "On the Method of Virtual Crack Extensions," International Journal of Numerical Methods in Engineering, Vol. 9, pp. 187-207, 1975.

¹⁴ Parks, D. M., "The Virtual Crack extension Method for Nonlinear Material Behavior," Computer Methods in Applied Mechanics and Engineering, Vol. 12, pp. 353-364, 1977.

¹⁵ de Koning, A. U. and C. Lof, "K-Distributions Extrapolated on the Basis of Stress Intensity Rates," Proceedings of the Third International Conference on Numerical Methods in Fracture Mechanics, eds. A. R. Luxmore and D. R. J. Owen, Pineridge Press Limited, Swansea, UK, 1984, p. 195.

de Koning, A. U., "Comparison of Some Methods to Calculate Stress Intensity Values from Results of Finite Element Analysis," Memorandum SC-78-170, The National Aerospace Laboratory of The Netherlands, Jan. 1979.

¹⁶ Rice, J. R., "An Examination of the Fracture Mechanics Energy Balance from the Point of View of Continuum Mechanics," Proceedings of the First International Conference on Fracture, Sendai, Japan, September 12-17, 1965, T. Yokobori, T. Kawasaki, and J. L. Swedlow, Eds. p. 309.

¹⁷ Rice, J. R., "A Path-Independent Integral and the Approximate Analyses of Strain Concentration by Notches and Cracks," Journal of Applied Mechanics, Vol. 35, 1968, pp. 376-386.

¹⁸ Bittencourt, T. N., A. Barry, and A. R. Ingraffea, "Comparison of Mixed Mode Stress-Intensity Factors Obtained Through Displacement Correlation, J-Integral Formulation, and Modified Crack-Closure Integral," Fracture Mechanics: Twenty-Second Symposium, Vol. II, ASTM STP 1131, S. N. Atluri, J. C. Newman, Jr., I. S. Raju, and J. S. Epstein, Eds., American Society for Testing and Materials, Philadelphia, 1992, pp. 69-82.

¹⁹ Rice, J. R., "An Examination of the Fracture Mechanics Energy Balance from the Point of View of Continuum Mechanics," Proceedings of the First International Conference on Fracture, Sendai, Japan, September 12-17, 1965, T. Yokobori, T. Kawasaki, and J. L. Swedlow, Eds. p. 309.

²⁰ Raju, I. S., and K. N. Shivakumar, "Implementation of Equivalent Domain Integral Method in the Two-Dimensional Analysis of Mixed-Mode Problems," NASA CD-181813, Apr. 1989.

²¹ Pickard, A. C., The Application of 3-Dimensional Finite Element Methods to Fracture Mechanics and Fatigue Life Prediction, Engineering Materials Advisory Services, LTD., West Midlands, UK, 1986, p. 70.

-
- ²² Irwin, G. R., Analysis of Stresses and Strains Near the End of a Crack Traversing a Plate," Journal of Applied Mechanics, Vol. 24, Trans. ASME, Vol. 1957, pp. 361-364.
- ²³ Rybicki, E. F. and M. F. Kanninen, "A Finite Element Calculation of Stress Intensity Factors by a Modified Crack Closure Integral," Engineering Fracture Mechanics, 9, 1977, pp. 931-938.
- ²⁴ Shivakumar, K. N., P. W. Tan, and J. C. Newman, Jr., "A Virtual Crack-Closure Technique for Calculating Stress Intensity Factors for Cracked Three Dimensional Bodies," International Journal of Fracture, 36, 1988, pp. R43-R50.
- ²⁵ K. N. Shivakumar and J. C. Newman, Jr., "ZIP3D - An Elastic and Elastic-Plastic Finite-Element Analysis Program for Cracked Bodies," Technical Memorandum NASA-TP-102753, Jun. 1990.
- ²⁶ Zienkiewicz, O. C. The Finite Element Method, Third Edition. New York: McGraw-Hill, 1979.
- ²⁷ Logan, Daryl L. A First Course in the Finite Element Method. Boston: PWS Publishers, 1986.
- ²⁸ Cook, Robert D. Concepts and Applications of Finite Element Analysis. New York: John Wiley & sons, 1981.
- ²⁹ Hughes, Thomas J. R. The Finite Element Method: Linear Static and Dynamic Finite Element Analysis. New Jersey, Prentice-Hall Inc., 1987.
- ³⁰ Zienkiewicz, O. C., R. L. Taylor, and J. M. Too, "Reduced Integration Techniques in General Analysis of Plates and Shells," International Journal of Numerical Methods in Engineering, Vol. 3, pp. 275-290, 1971.
- ³¹ Iron, B. N. and T. K. Hellen, "On Reduced Integration in Solid Isoparametric Elements When Used in Shells with Membrane Modes," International Journal of Numerical Methods in Engineering, vol. 10, pp. 1179-1182, 1975-1976.
- ³² Boresi, Arthur P. and Omar M. Sidebottom, Advanced Mechanics of Materials 4th Edition, John Wiley and Sons, New York, 1985, p. 570.
- ³³ Sneddon, I. N., The Distribution of Stress in the Neighbourhood of a Crack in an Elastic Solid," Proceedings of the Royal Society London A 187, 1946, pp. 229 - 260, qtd. in Broek, D. Elementary Engineering Fracture Mechanics. Martinus Nijhoff Publishers, Dordrecht, 1986, p. 88.
- ³⁴ Newman Jr., J. C. Personal Interview. 02 Feb. 1996.
- ³⁵ Newman, Jr., J. C. and I. S. Raju, "Stress-Intensity Factor Equations for Cracks in Three-Dimensional Finite Bodies Subjected to Tension and Bending Loads,"

Computational Methods in the Mechanics of Fracture, Volume 2, Satya N. Atluri editor, North-Holland, Amsterdam, 1986.

³⁶ Green, A. E. and I. N. Sneddon, "The Stress Distribution in the Neighbourhood of a Flat Elliptical Crack in an Elastic Solid," Proceedings Cambridge Phil. Soc., 46 (1950) pp. 159-164.

³⁷ Schijve, J., "Brief Note on the Stress Intensity Factor for Elliptical Crack," Engineering Fracture Mechanics, Vol. 18, No. 5, 1983, pp. 1067-1069.

³⁸ Newman Jr., J. C., "An Improved Method of Collocation for the Stress Analysis of Cracked Plates with Various Shaped Boundaries," NASA Technical Note TN-6376, Aug. 1971.

³⁹ NASGRO Fatigue Crack Growth Computer Program, Version 2.01, NASA JSC-22267A, May 1994.

⁴⁰ Roberts, R. and T. Rich, "Stress Intensity Factors for Plate Bending," Transactions of ASME, Journal of Applied Mechanics, Vol. 34, No. 3, Sep. 1967, pp. 777-779.

⁴¹ Roberts, Richard, and John J. Kibler, "Some Aspects of Fatigue Crack Propagation," Engineering Fracture Mechanics, Vol. 2., 1971, pp. 243-260.

⁴² Shivakumar, V. and R. G. Forman, "Green's Function for a Crack Emanating from a Circular Hole in an Infinite Sheet," International Journal of Fracture, Vol. 16, No. 4, Aug. 1980, pp. 305-316.

⁴³ Shivakumar, V. and Y. C. Hsu, "Stress Intensity Factors for Cracks Emanating from the Loaded Fastener Hole," Presented at the International Conference on Fracture Mechanics and Technology, Hong Kong, Mar. 1977.

⁴⁴ Tweed, J. and D. P. Rooke, "The Distribution of Stress Near the Tip of a Radial Crack at the Edge of a Circular Hole," International Journal of Engineering Science, Vol. 11, 1973, pp. 1185-1195.

⁴⁵ Murakami, Y., Stress Intensity Factors Handbook, Volume 3, The Society of Materials Science, Japan, Pergamon Press, Tokyo, pp. 607-610.

⁴⁶ Miyoshi, T., K. Ishii, and S. Yoshida, "Database of Stress Intensity Factors for Surface Cracks in Pre/Post Penetration," Transactions of Japanese Society of Mechanical Engineers, Vol. 56, No. 527 (1990), pp. 1563-1569. qtd. in Murakami, Y., Stress Intensity Factors Handbook, Volume 3, The Society of Materials Science, Japan, Pergamon Press, Tokyo, pp. 607-610.

⁴⁷ Miyoshi, T. and S. Yoshida, "Analysis of Stress Intensity Factors for Surface Cracks in Pre/Post Penetration," Transactions of Japanese Society of Mechanical Engineers, Vol. 54, No. 505 (1988), pp. 1771-1777. qtd. in Murakami, Y., Stress Intensity Factors Handbook, Volume 3, The Society of Materials Science, Japan, Pergamon Press, Tokyo, pp. 607-610.

-
- ⁴⁸ Irwin, G. R., "The Crack Extension Force for a Part-Through Crack in a Plate," Journal of Applied Mechanics, Vol. 29, Trans. ASME, 1962, pp. 651-654.
- ⁴⁹ Newman, Jr., J. C. and I. S. Raju, "Stress-Intensity Factor Equations for Cracks in Three-Dimensional Finite Bodies Subjected to Tension and Bending Loads," Computational Methods in the Mechanics of Fracture, Volume 2, Satya N. Atluri editor, North-Holland, Amsterdam, 1986.
- ⁵⁰ Bowie, O. L., "Analysis of an Infinite Plate Containing Radial Cracks Originating at the Boundary of an Internal Circular Hole," Journal of Mathematics and Physics, Vol. 35, 1960, pp. 60-71.
- ⁵¹ Tada, Hiroshi, Paul C. Paris, and George R. Irwin, The Stress Analysis of Cracks Handbook, 2ND Edition, Paris Productions Incorporated and Del Research Corporation, St. Louis, 1985.
- ⁵² Broek, D. Elementary Engineering Fracture Mechanics. Martinus Nijhoff Publishers, Dordrecht, 1986.
- ⁵³ Shah, R. C., "Stress Intensity Factors for Through and Part Through Cracks Originating at Fastener Holes," Mechanics of Crack Growth, ASTM STP 590, American Society for Testing and Materials, 1976, pp. 429-459.
- ⁵⁴ Chang, Fu-Kuo, Richard A. Scott, and George S. Springer, "Strength of Mechanically Fastened Composite Joints," Journal of Composite Materials, Vol. 16, No. 6, Nov. 1982, pp. 470-494.
- ⁵⁵ Crews, John H., C. S. Hong, and I. S. Raju, "Stress Concentration Factors for Finite Orthotropic Laminates with a Pin-Loaded Hole," NASA TP-1862, 1981.
- ⁵⁶ de Jong, Theo, "Stresses Around Pin-Loaded Holes in Elastically Orthotropic or Isotropic Plates," Journal of Composite Materials, Vol. 11, Jul. 1977, pp. 313-331.
- ⁵⁷ Eshwar, V. A., B. Dattaguru, and A. K. Rao, "Partial Contact and Friction in Pin Joints," Report No. ARDB-STR-5010, Department of Aeronautical Engineering, Indian Institute of Science, Dec. 1977.
- ⁵⁸ Newman, Jr., J. C., Electronic Communication, NASA Langley Research Center, 21 Feb. 1996.

